



High metabolic zinc demand within native Amundsen and Ross sea phytoplankton communities determined by stable isotope uptake rate measurements

Riss M. Kell^{1,4,i}, Rebecca J. Chmiel¹, Deepa Rao¹, Dawn M. Moran¹, Matthew R. McIlvin¹, Tristan J. Horner¹, Nicole L. Schanke³, Ichiko Sugiyama¹, Robert B. Dunbar², Giacomo R. DiTullio³, and Mak A. Saito¹

¹Department of Marine Chemistry and Geochemistry, Woods Hole Oceanographic Institution, Woods Hole, MA 02543, USA

²Doerr School of Sustainability, Stanford University, Stanford, CA 94305, USA

³Hollings Marine Laboratory, College of Charleston, Charleston, SC 29412, USA

⁴Gloucester Marine Genomics Institute, Gloucester, MA 01930-3006, USA

ⁱpreviously published under the name Riss Kellogg

Correspondence: Mak A. Saito (msaito@whoi.edu)

Received: 5 July 2024 – Discussion started: 2 August 2024

Revised: 2 November 2024 – Accepted: 5 November 2024 – Published: 19 December 2024

Abstract. Zinc (Zn) is an essential micronutrient for most eukaryotic phytoplankton. Zn uptake by phytoplankton within the euphotic zone results in nutrient-like dissolved Zn (dZn) profiles with a large dynamic range. The combination of key biochemical uses for Zn and large vertical gradients in dZn implies the potential for rapid rates of Zn removal from the surface ocean. However, due to the ease of contamination at sea, direct measurements of dZn uptake within natural environments have not been previously made. To investigate the demand for dZn and for dissolved cadmium (dCd; a closely related nutrient-like element) within Southern Ocean phytoplankton communities, we conducted ⁶⁷Zn and ¹¹⁰Cd tracer uptake experiments within the Amundsen Sea, Ross Sea, and Terra Nova Bay of the Southern Ocean. We observed a high magnitude of Zn uptake ($\rho\text{Zn} > 100 \text{ pmol dZn L}^{-1} \text{ d}^{-1}$) into the particulate phase that was consistent with ambient depleted dZn surface concentrations. High biomass and low partial pressure of carbon dioxide in seawater (seawater $p\text{CO}_2$) appeared to contribute to ρZn , which also led to increases in ρCd likely through the upregulation of shared transport systems. These high ρZn measurements further imply that only short timescales are needed to deplete the large winter dZn inventory down to the observed surface levels in this important carbon-capturing region. Overall, the high magnitude of Zn uptake into the particulate fraction suggests that even in the Zn-rich waters of the Southern Ocean, high

Zn uptake rates can lead to Zn depletion and potential Zn scarcity.

1 Introduction

Zinc (Zn) is an essential trace metal micronutrient for marine phytoplankton with roles in carbon fixation, organic phosphorus uptake, and transcriptional and translational processes, among others (Morel et al., 2013, 2020; Shaked et al., 2006; Twining and Baines, 2013). Nutrient-like depth profiles of total dissolved Zn (dZn) are characterized by depleted surface concentrations due to uptake by phytoplankton within the euphotic zone, reflecting this high biological demand (Fitzwater et al., 2000; Lohan et al., 2002; Midgag et al., 2019; Zhao et al., 2014). Zn is particularly important as a catalytic cofactor in carbonic anhydrase (CA) metalloenzymes, which catalyze the reversible dehydration of HCO_3^- to CO_2 . As HCO_3^- constitutes about 90 % of the dissolved inorganic carbon (DIC) pool in the surface ocean, CAs in marine algae are a critical part of the carbon-concentrating mechanism (CCM) that maintains a CO_2 supply to the carbon-fixing enzyme ribulose-1,5-biphosphate carboxylase/oxygenase (RUBISCO). Less abundant divalent metal cations such as cobalt (Co^{2+}) and cadmium (Cd^{2+}) can replace Zn^{2+} in some algal CA subtypes (Lane et al., 2005),

conferring biochemical flexibility to algae confronted with low Zn bioavailability.

While Cd is known to cause toxic effects in most organisms (Brand et al., 1986; Das et al., 1997), dissolved cadmium (dCd) depth profiles are also nutrient-like. As noted above, the biological use of Cd as a catalytic cofactor within Cd-containing carbonic anhydrase (ζ -CA, or CDCA) likely contributes to surface dCd depletion and thus to the observed nutrient-like profiles, though this remains the only known biological use of Cd to date (Haas et al., 2009; Lee and Morel, 1995; Sunda and Huntsman, 2000). It has also been proposed that phytoplankton may assimilate Cd abiotically – this mode of Cd uptake is nonspecific, a case of “mistaken identity” in which phytoplankton bind and store imported Cd inside the cell to avoid toxicity, coupling the cycling of Cd to the biological cycle of nutrients (Horner et al., 2013). As the beneficial effect of adding Cd to phytoplankton cultures has only been observed when Zn is limiting (Lee et al., 1995; Price and Morel, 1990; Xu et al., 2007), it has been speculated that the ability to use Cd in place of Zn in CDCA may confer a competitive advantage to Zn-limited algae under low pCO₂. To date, homolog *cdca* genes have been found exclusively in diatom species (Park et al., 2007, 2008). However, since the beneficial effect of Cd has also been observed in organisms such as the green alga *Tetraselmis maculata* and the coccolithophore *Emiliania huxleyi* that lack the *cdca* gene (Lee and Morel, 1995), it is thought that Cd may have other biochemical functions in phytoplankton still awaiting discovery.

Due to the generally high (> 1 nM) dZn concentrations observed in Southern Ocean waters (Baars and Croot, 2011), Zn has not been considered to be a limiting micronutrient in this region, despite the fact that Southern Ocean diatom species possess cellular Zn quotas that are 3–15× higher compared to those of low-latitude species (Twining and Baines, 2013), with model-inferred Zn uptake rates used to find that Southern Ocean phytoplankton account for 62 % of global Zn uptake (Roshan et al., 2018). Substantial removal of dZn from Southern Ocean surface waters appears associated with high biomass blooms and low pCO₂ conditions during austral spring and summer, creating the potential for phytoplankton growth to become Zn and carbon co-limited (Kell et al., 2023; Morel et al., 1994). While phytoplankton growth in the Southern Ocean is well known to be primarily limited by Fe availability (Arrigo et al., 2008; Martin, 1990), melting icebergs and ice shelves are known to act as external sources of Fe (Hopwood et al., 2019; Person et al., 2021; Planquette et al., 2013; St-Laurent et al., 2017) with larger Fe inputs expected from increased ice melt in a warming climate. The majority of ice-melted Fe input is sourced from particulate lithogenic material (entrained during grounding of ice shelves on the continent and sediments). Fe in crustal material is more abundant than Zn (3.5 % as Fe versus 0.0071 % as Zn) (Taylor and McLennan, 1985), creating a large inventory of particulate Fe available that can be partially dissolved by biotic and abiotic processes. Increased dissolved

Fe (dFe) inputs to surface Antarctic waters may act to relieve Fe stress but would simultaneously support the development of other nutrient limitations. For example, low availabilities of both dZn and vitamin B₁₂ have been previously observed to co-limit phytoplankton growth with Fe in the Ross Sea (Bertrand et al., 2007; Kell et al., 2023). A high demand for Zn naturally exists within eukaryotic phytoplankton due to the requirement for Zn²⁺ in numerous metabolic functions; therefore, without similarly enhanced inputs of dZn to the water column, the alleviation of primary Fe limitation could induce Zn stress as the next most in-demand metal micronutrient. Coastal polynyas that form within the Amundsen and Ross seas during austral spring and summer are particularly primed to experience Zn stress as these regions host highly productive seasonal phytoplankton blooms that act as significant carbon sinks (Arrigo et al., 2012). This high productivity draws pCO₂ down to low levels (< 200 ppm), putting pressure on the carbon-concentrating mechanism of photosynthetic phytoplankton to acquire CO₂ and thus to acquire Zn as the predominantly utilized metal cofactor within carbonic anhydrases.

The present study enhances our knowledge of the rate of dZn removal from the surface Southern Ocean and uptake into the particulate fraction with empirical field data measured within native Southern Ocean phytoplankton communities. This study developed a field-based, stable Zn isotope uptake rate method, building on a prior stable Cd uptake rate method (Cox et al., 2014). While Zn uptake has been measured in laboratory cultures (Sunda and Huntsman, 1992, 1995, 2000), and the influence of grazing and tropic transfer studies have been conducted using radioactive isotopes (Hutchins and Bruland, 1995, 1994), to our knowledge direct measurements of Zn uptake in natural marine phytoplankton communities have not been conducted previously, despite interest in modeling the biogeochemical uptake and cycling of Zn (Weber et al., 2018). We measured the total uptake rates of Zn and Cd along the shelves of the Amundsen Sea and Ross Sea during the austral summer of 2017–2018 (December–March). This was accomplished by introducing ⁶⁷Zn and ¹¹⁰Cd (with natural abundances of 4.10 % and 12.5 %, respectively) into short-term (24 h) incubation experiments. The aim was to quantify the transfer of dissolved ¹¹⁰Cd²⁺ and ⁶⁷Zn²⁺ into the particulate fraction exceeding 3 μm. Both stable isotopes can be used as uptake tracers by analysis of isotope abundances that deviate from natural abundances within the particulate phase. The transfer of added isotopes into the particulate phase is the combined result of (1) active transport of metal into cells, (2) nonspecific metal adsorption to cell surfaces, (3) metal adsorption to non-living particulate organic matter, and (4) metal adsorption to particulate inorganic matter, though we expect active transport into cells to dominate the measured particulate isotopic signal due to the high abundance of actively growing autotrophic cells in the photic zone observed in the Southern Ocean during austral summer. These measurements of uptake

rates were then used to infer timescales of surface dZn depletion in these Antarctic environments. These uptake rates contribute to understanding the biological demand and potential for Zn limitation of primary productivity in highly productive coastal environments, such as the polynyas surrounding Antarctica (Kell et al., 2023).

2 Methods

2.1 Study area and sample collection

Samples were collected during the CICLOPS (Cobalamin and Iron Co-Limitation of Phytoplankton Species) expedition (NBP18-01) aboard the RVIB *Nathaniel B. Palmer*, 11 December 2017–3 March 2018, in the Amundsen Sea and Ross Sea of the Southern Ocean (Fig. 1). Station metadata are given in Table S1 in the Supplement. Water samples were collected using trace metal clean (TMC) sampling protocols described previously (Cutter and Bruland, 2012). A TMC rosette suspended on a Kevlar line and equipped with 12 total 8 L X-Niskin bottles (Ocean Test Equipment) was used to collect seawater at depths ranging from 10–600 m. Continuous underway measurements of pCO₂ at ~ 5 m depth were taken using a pCO₂ measurement system from Lamont–Doherty Earth Observatory (LDEO, 0.017 s⁻¹ rate). Hydrography data were collected using sensors deployed on a titanium trace metal rosette (TMR) in tandem with TMC Niskin bottles. The TMR was equipped with sensors to measure temperature, conductivity, pressure, dissolved oxygen, chlorophyll (Chl) fluorescence, altimetry, beam transmission, and photosynthetically active irradiance (PAR). Chl fluorescence was measured using a Wet-Labs ECO-FL fluorometer. A complete data report and sensor list are available at <https://service.rvdata.us/data/cruise/NBP1801/doc/NBP1801DATA.pdf> (last access: 14 December 2024) (<https://www.rvdata.us/>, last access: 14 December 2024). Mixed-layer depth (MLD) was determined for each station within Terra Nova Bay as the first depth at which the difference between the potential density (σ_{θ}) and reference density (the potential density at 10 m, σ_{ref}) was greater than or equal to 0.125 kg m⁻³ (Bishop and Wood, 2009; Ohnemus et al., 2017).

2.2 Preparation of plasticware

Polyethylene and polycarbonate sampling and incubation bottles were rigorously cleaned to remove trace metal contaminants before use. Bottles were rinsed with Milli-Q water (Millipore), soaked for 72 h in < 1 % Citranox detergent, rotated, soaked for an additional 72 h, and then rinsed five times with Milli-Q water. Bottles were then filled with 10 % HCl (Baker Instra-Analyzed) by volume and soaked for a minimum of 1 week, rotated, and soaked for another week. Bottles were then rinsed five times with dilute acid (HCl, pH 2) and stored double-bagged in plastic zip bags. All cleaning

work was conducted in a Class 100 clean room. Polypropylene 15 mL centrifuge tubes used in sample processing were cleaned of potential metal contamination by soaking in 10 % HCl for 5 d and rinsing with pH 2 HCl prior to use.

2.3 Sampling for total dissolved metal analyses

Samples for the analysis of total dissolved Zn, Cd, Fe, Mn, Cu, and Ni concentrations were collected shipboard by pressure-filtering X-Niskin bottles through an acid-washed 142 mm, 0.2 μM Supor membrane filter (Pall) within 3 h of rosette recovery using high-purity (99.999 %) N₂ gas. Total dissolved water samples were collected into 250 mL TMC polyethylene bottles and stored double-bagged in plastic zip bags. Seawater samples for ¹¹⁰Cd and ⁶⁷Zn stable isotope uptake experiments were collected in the same way but without filtering. All sample collection occurred shipboard within a TMC van containing laminar flow hoods and plastic sheeting. Samples for total dissolved metal analysis were acidified to pH 1.7 with high-purity HCl (Optima, Fisher Scientific) within 7 months of sampling and were stored acidified at room temperature for over 1 year prior to analysis.

2.4 Analyses of total dissolved metals using isotope dilution

Quantification of dissolved metals in samples and reference seawater was performed for total dissolved Fe, Ni, Cu, Zn, and Cd using isotope dilution. Following this, 15 mL of acidified seawater sample was spiked with 50 μL of a stable isotope spike solution artificially enriched in ⁵⁷Fe, ⁶¹Ni, ⁶⁵Cu, ⁶⁷Zn, and ¹¹⁰Cd (“spike isotopes”). Reference isotopes used in this study were ⁵⁶Fe, ⁶⁰Ni, ⁶³Cu, ⁶⁶Zn, and ¹¹⁴Cd. All spike isotopes were received in solid form (Oak Ridge National Laboratory). Initial dissolution and all subsequent dilutions were made using concentrated nitric acid (Optima, Fisher Scientific). Concentrations and ratios of isotopes for each metal in the spike solution were verified by inductively coupled plasma mass spectrometry (ICP-MS) using a multi-element standard curve (SPEX CertiPrep). The composition of the isotope spike addition was made such that the target isotope ratios in the total 15 mL spiked sample would be ⁵⁷Fe/⁵⁶Fe = 0.7, ⁶¹Ni/⁶⁰Ni = 0.5, ⁶⁵Cu/⁶³Cu = 1, ⁶⁷Zn/⁶⁶Zn = 0.7, and ¹¹⁰Cd/¹¹⁴Cd = 1 and were verified with ICP-MS. These ratios were chosen to minimize the uncertainty introduced by error propagation through the isotope dilution equation (Kato et al., 1990; Rudge et al., 2009; Tan et al., 2020; Wu and Boyle, 1998). The same spike solution was used to spike all samples from all depths. Because it is monoisotopic, total dissolved Mn was calculated using a

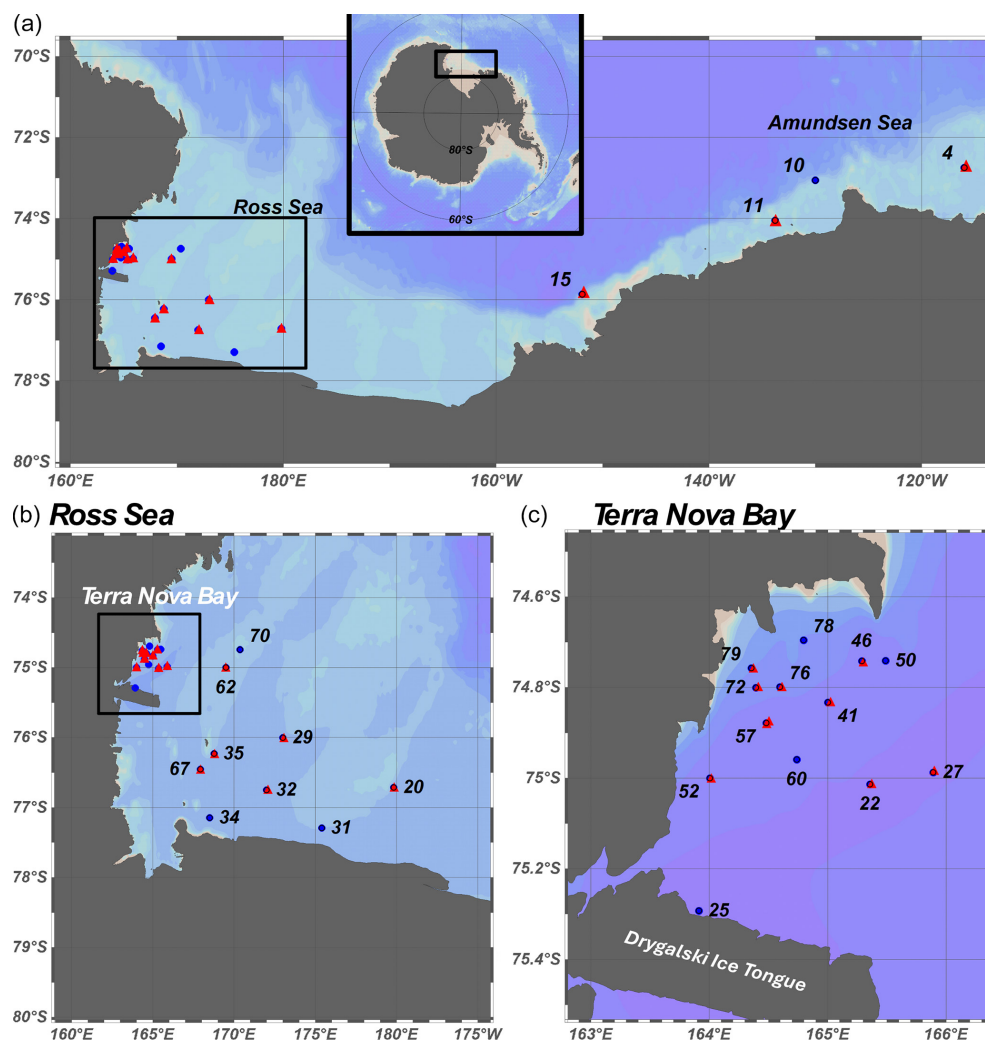


Figure 1. (a) Map showing the stations sampled over the course of the CICLOPS cruise. Stations marked by red triangles indicate those at which stable ^{67}Zn and ^{110}Cd uptake rate experiments were performed. An expanded map of stations sampled in the Ross Sea is shown in panel (b), while a further expansion of stations sampled in Terra Nova Bay is shown in panel (c).

modified isotope dilution equation:

$$\begin{aligned} \text{Mn}(\text{nM}) &= \frac{{}^{55}\text{Mn}_{\text{spl}}(\text{cps})}{{}^{57}\text{Fe}_{\text{spl}}(\text{cps})} \times {}^{57}\text{Fe}_{\text{spike}}(\text{nM}) \\ &\times {}^{57}\text{Fe}_{\text{slope}}(\text{cps ppb}^{-1}) \\ &\times \frac{1}{{}^{55}\text{Mn}_{\text{slope}}(\text{cps ppb}^{-1})}, \end{aligned} \quad (1)$$

in which ${}^{55}\text{Mn}_{\text{spl}}$ and ${}^{57}\text{Fe}_{\text{spl}}$ refer to the blank-corrected counts per second (cps) of ${}^{55}\text{Mn}$ and ${}^{57}\text{Fe}$ in the spiked sample, ${}^{57}\text{Fe}_{\text{spike}}$ is the concentration of ${}^{57}\text{Fe}$ in the spike, ${}^{57}\text{Fe}_{\text{slope}}$ is the slope of the external standard calibration curve (SPEX curve) relating ${}^{57}\text{Fe}$ cps to ppb, and ${}^{55}\text{Mn}_{\text{slope}}$ is the slope of the external calibration curve (SPEX curve) relating ${}^{55}\text{Mn}$ cps to ppb. Due to the acidification of seawater prior to ICP-MS analysis, Mn ICP-MS measurements do not include contributions from humic-type Mn(III)-ligand com-

plexes (Oldham et al., 2021). Until the inclusion of Mn(III) is resolved and intercalibrated, we report these Mn values as Mn(II) and note that they are consistent with prior studies employing the same acidification technique (Gerringa et al., 2020; Noble et al., 2013; Sedwick et al., 2000).

Preconcentration of spiked seawater samples for total dissolved metal analysis was performed using the automated solid-phase extraction system seaFAST-pico (Elemental Scientific) in offline concentration mode with an initial volume of 15 mL and elution volume of 500 μL (Bown et al., 2017; Jackson et al., 2018; Rapp et al., 2017; Wuttig et al., 2019). The seaFAST contains a NOBIAS-chelate PA1 resin column (ethylenediaminetriacetate and iminodiacetate) suitable for the simultaneous preconcentration of several trace metals (Fe, Mn, Zn, Cu, Co, Cd, Ni) with high sensitivity and quantitative recovery (Billler and Bruland, 2012; Sohrin et al., 2008).

Adjusted seaFAST software settings were a 17 s load loop time and a single 10 mL load cycle.

Reagents consisted of a 1.5 M ammonium acetate pH 6.0 buffer made using glacial acetic acid and ammonium hydroxide (20 %–22 %) of the highest purity (Optima grade, Fisher Chemical), a 1 % nitric acid rinse solution (Optima grade, Fisher Chemical), and a 10 % nitric acid elution buffer (Optima grade, Fisher Chemical) with 10 ppb indium (^{115}In , SPEX CertiPrep) added as an internal standard. Solutions were prepared with 18.2 Ω Milli-Q water (Millipore).

Following offline seaFAST preconcentration, multi-elemental quantitative analysis was performed using an iCAP-Q inductively coupled plasma-mass spectrometer (Thermo Scientific). To minimize oxide interference on metal isotopes, a cooled spray chamber and helium collision gas were employed. Analytes were measured in single quadrupole mode (kinetic energy discrimination, KED). Concentrations of Mn, Fe, Ni, Cu, Zn, and Cd were determined using a six-point external standard curve of a multi-element standard (SPEX CertiPrep), diluted to range from 1–10 ppb in 5 % nitric acid. An indium standard (SPEX CertiPrep) was similarly added to these standard stocks, diluted to a range of 1–10 ppb. Instrument injection blanks consisted of 5 % nitric acid in Milli-Q. Standard curve R^2 values were ≥ 0.98 for all metals monitored. Method accuracy and precision were assessed using the 2009 GEOTRACES coastal surface seawater (GSC) standard ($n = 8$; Table S2), which produced values consistent with consensus results.

2.5 Procedural blanks and limit of detection (LOD)

Procedural blanks were quantified by pre-concentrating 30 mL of Milli-Q water adjusted to pH 2 with HCl (Optima, Fisher Scientific) to 1 mL. Metal concentrations were determined using an external SPEX multi-element standard as described above. The LOD was calculated as $3 \times$ the standard deviation of the blank measurements (13.5 pM Fe, 2.9 pM Ni, 1.6 pM Cu, 38.1 pM Zn, and 0.3 pM Cd).

2.6 Uptake experiments: ^{67}Zn and ^{110}Cd spiking, incubation, and sample collection

The ^{67}Zn and ^{110}Cd stable isotope uptake experiments were modeled after those conducted by Cox et al. (2014), with the addition of Zn uptake measurements. An overall schematic detailing these experiment workflows is shown in Fig. 2. Uptake experiments were performed at 18 stations total (Fig. 1). Raw (unfiltered) seawater was collected shipboard over a depth range of 10–600 m into 250 mL TMC polycarbonate incubation bottles. All incubation bottles were filled with minimal headspace such that the total culture volume was ~ 275 mL. Two incubation bottles per depth were filled with raw seawater – one was spiked with ^{67}Zn , the other was spiked with ^{110}Cd . The Cd and Zn isotope spikes were prepared by dissolving ^{110}CdO and ^{67}ZnO (Oak Ridge National

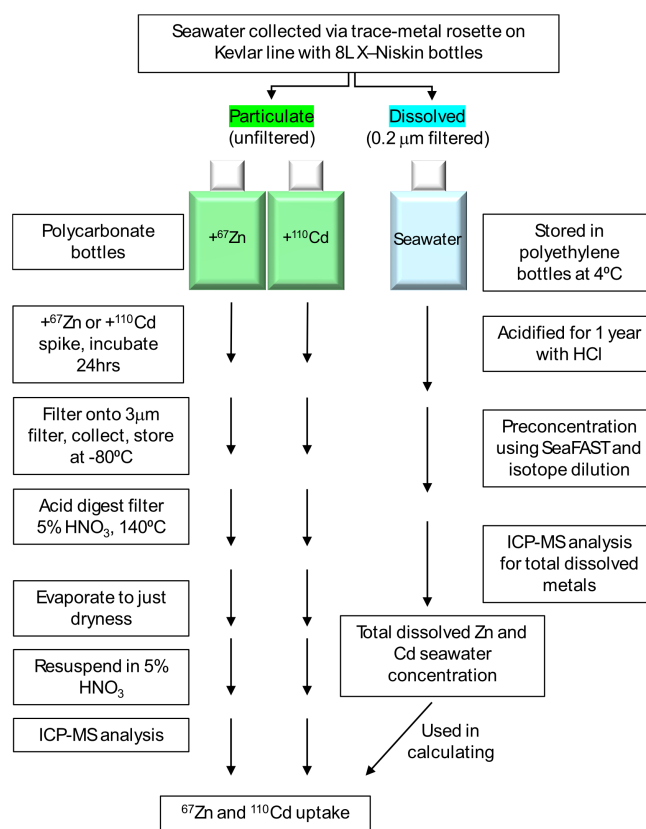


Figure 2. Diagram showing the overall workflow used to measure particulate uptake of ^{110}Cd and ^{67}Zn and total dissolved Cd and Zn, after Cox et al. (2014).

Laboratory) in 5 % HNO_3 (Seastar Baseline) and were diluted using Milli-Q water to minimize added acidity. When added to the filled incubation bottles, the total added (spiked) concentration of Cd was 300 pM and the total added concentration of Zn was 2 nM. The chosen total added concentrations were based on the surface ratio of total dissolved Cd (dCd) to total dissolved Zn (dZn) reported previously for the Ross Sea (Fitzwater et al., 2000). Immediately after spiking, incubation bottles were sealed, inverted to mix, and transferred to flow-through on-deck incubators for 24 h. Incubators were shielded by black net neutral density screening to allow 20 % ambient light penetration.

Biomass was collected after 24 h by vacuum filtering the entire volume of each incubation sample at 34.5 kPa (5 psi) onto an acid-cleaned 3 μm , 50 mm acrylic copolymer (Versapore) filter (Pall) mounted on an acid-cleaned Teflon (Savillex) filtration rig. Samples were filtered through 3 μm pore-size filters rather than 0.2 μm in order to minimize filtration time (and thus time exposed to potential contamination) and to capture the bulk of eukaryotic phytoplankton biomass typically found in the Southern Ocean. An aliquot of 1 mL of 0.2 μm filtered surface seawater (collected at 10 m depth) was used to rinse the sample before collecting the filter into

an acid-cleaned 2 mL cryovial using acid-rinsed plastic forceps. Filter blanks were duplicate 3 µm acid-cleaned Versapore (Pall) filters that were placed onto the filtration rig, rinsed with filtered surface seawater, collected, stored, and processed as samples to correct for any contaminating metals present on the filters themselves. Blanks were collected at each station. Filters were stored frozen at -80°C in acid-cleaned cryovials until analysis. The filtration rig was rinsed with pH 2 HCl between samples. Polycarbonate incubation bottles were cleaned between stations with a 10 % HCl rinse and several rinses in Milli-Q water, followed by a brief soak in 10 % HCl followed by a pH 2 HCl rinse. All spike addition and sample filtration procedures were completed in a fabricated shipboard positive-pressure clean-room environment made of laminar flow hoods and plastic sheeting.

We note that the total Zn and Cd uptake rate values presented in this study represent potential uptake rates rather than true uptake rates. This naturally arises as a consequence of adding the spiked tracer ^{67}Zn and ^{110}Cd into raw surface seawater. As this seawater is naturally depleted in both metals, the spike addition artificially increases the total Zn and Cd present and thus could perturb the response of biology to these additions. It should also be noted that both ^{67}Zn and ^{110}Cd spikes were not equilibrated with natural seawater before their addition to incubation bottles to maintain experimental consistency. Experiments of this nature have been conducted previously using radioisotopes as tracers (Cullen et al., 1999; Hutchins et al., 1999; Morel et al., 1994; Sunda and Huntsman, 1995), though we chose to use stable isotopes for ease of shipboard use and waste disposal.

2.7 Filter digestion and particulate ICP-MS analysis

All work was performed in a Class 100 clean room under laminar flow hoods. Sample filters were retrieved from storage at -80°C , removed from cryovials using plastic acid-washed forceps, and transferred into trace metal clean 15 mL PFA vials with 4 mL of 5 % HNO_3 (Optima) containing a 1 ppb Indium (In) internal standard. Filters were digested for ~ 3.5 h at 140°C using a HotBlock[®] heating block (Environmental Express, USA). Filters were then removed and discarded, leaving behind the liquid extract. After evaporating the remaining solution to just dryness, the residue was resuspended in 2 mL of 5 % HNO_3 (Optima) by light vortexing. Process blank filters were digested and processed in the same way as sample filters. Digests were analyzed in duplicate by ICP-MS using a Thermo ICAP-Q plasma mass spectrometer calibrated to a multi-element standard curve (SPEX Certiprep) over a range of 1–20 ppb. Duplicate values were in good agreement (File 1 in the Supplement), and the average value was used in further calculations. Natural Cd and Zn isotope abundances of the standards were assumed to calculate concentrations of ^{110}Cd , ^{111}Cd , ^{114}Cd , ^{67}Zn , ^{66}Zn , and ^{68}Zn . Digests were analyzed in KED mode after an 85 s sample uptake window, and element mass windows were scanned

three times during measurements. The 1 ppb In internal standard was used to correct for variation in sample delivery and plasma suppression between samples. Process blanks were subtracted from measured sample concentrations. Phosphorus concentrations were simultaneously measured by ICP-MS and were calibrated to a standard curve ranging from 100–3200 ppb using a 1 ppm certified P stock (Alfa Aesar Specpure). Equation (2) was used for the calculations described above:

$$M_{\text{particulate}} = \left[\frac{M_{\text{sample}}}{I_{\text{sample}}} - \frac{M_{\text{blank}}}{I_{\text{blank}}} \right] \times \frac{I_{\text{digestion}}}{M_{\text{slope}}} \times \frac{V_{\text{digested}}}{V_{\text{filtered}}}, \quad (2)$$

where V_{filtered} is the total spiked sample volume estimated to have passed through the filter (275 mL), V_{digested} is the final volume the sample was resuspended in (2.0 mL), M_{sample} is the metal of interest measured in the sample in units of counts per second (cps), M_{blank} is the metal of interest measured in the process blanks (cps), M_{slope} is the slope of the metal of interest obtained by the standard curve (cps ppb^{-1}), I_{sample} is the In measured in the sample (cps), I_{blank} is the In measured in the process blanks (cps), $I_{\text{digestion}}$ is the cps of In measured in the 5 % HNO_3 + 1 ppb In digestion solution, and $M_{\text{particulate}}$ is the calculated concentration of the metal of interest in ppb ($\mu\text{g L}^{-1}$). This equation is the same as that used by Noble et al. (2013) for the determination of particulate metal concentrations using ICP-MS (Noble et al., 2013).

The Zn spike and Cd spike were also analyzed by ICP-MS using a 10-fold dilution of spike solution into 5 % HNO_3 containing 1 ppb In to determine isotopic compositions and concentrations. When added to filled incubation bottles (275 mL total volume), the added concentrations were 288 pM ^{110}Cd , 4.51 pM ^{111}Cd , and 1.69 pM ^{114}Cd for Cd-spiked bottles and 1.91 nM ^{67}Zn , 0.045 nM ^{66}Zn , and 0.047 nM ^{68}Zn for Zn-spiked bottles (Table S3). For all stations and all depths, ^{67}Zn and ^{110}Cd spike concentrations exceeded natural dissolved ^{67}Zn and ^{110}Cd concentrations, estimated by multiplying the total dissolved Zn and Cd by the natural isotope abundance of ^{67}Zn and ^{110}Cd (0.0410 and 0.1249, respectively; see comparisons in Fig. S2).

2.8 Calculating zinc and cadmium uptake using ^{67}Zn and ^{110}Cd

Total Zn and Cd uptake was calculated using Eqs. (3) and (4), respectively. The $^{110}\text{Cd}_{\text{Sample}}$ and $^{67}\text{Zn}_{\text{Sample}}$ values are the particulate ^{110}Cd and ^{67}Zn measured by ICP-MS analysis of the 3 µm sample filter (using the digestion protocol described in Sect. 2.7) normalized to the total culture volume (275 mL) and 24 h of incubation. The $^{110}\text{Cd}_{\text{Sample}}$ and $^{67}\text{Zn}_{\text{Sample}}$ values already in the particulate fraction (i.e., the pCd and pZn that existed in the water column upon collection of the raw seawater samples) were accounted for by subtracting these pre-existing particulate ^{110}Cd and ^{67}Zn values, i.e., $^{110}\text{Cd}_{\text{PEP}}$ and $^{67}\text{Zn}_{\text{PEP}}$. The pre-existing particulate value for ^{110}Cd was obtained from incubation bottles that had Zn

added but no Cd spike. Likewise, the pre-existing particulate value for ^{67}Zn was obtained from incubation bottles that had Cd added but no Zn spike. The ^{67}Zn spike solution was confirmed to contain virtually no ^{110}Cd , ^{111}Cd , or ^{114}Cd . The ^{110}Cd spike was likewise confirmed to contain virtually no ^{67}Zn , ^{64}Zn , or ^{66}Zn . As a result, we assumed that the added ^{67}Zn spike did not affect the pre-existing Cd and that the ^{110}Cd spike did not affect the pre-existing Zn. It is assumed that the pre-existing particulate blank was in steady state, meaning that it represented the Cd or Zn already in the particulate fraction and that any possible natural uptake that could occur during incubation for 24 h was negligible. The total dissolved pool of each metal isotope (denominator of each equation) is the sum of the dissolved ^{110}Cd or ^{67}Zn added as the spike ($^{110}\text{Cd}_{\text{Spike}}$, $^{67}\text{Zn}_{\text{Spike}}$) plus the natural, pre-existing dissolved ^{110}Cd or ^{67}Zn that was in the raw seawater ($^{110}\text{Cd}_{\text{Natural}}$, $^{67}\text{Zn}_{\text{Natural}}$) collected at each depth. To calculate $^{110}\text{Cd}_{\text{Natural}}$ and $^{67}\text{Zn}_{\text{Natural}}$, the total dissolved Cd or Zn measured by isotope dilution-ICP-MS (Cd_{Total} , Zn_{Total}) was multiplied by the natural abundance of ^{110}Cd and ^{67}Zn (12.49 % and 4.10 %, respectively). Dividing the particulate ^{110}Cd and ^{67}Zn by the total dissolved ^{110}Cd and ^{67}Zn yields the fraction of these metal isotopes that moved from the dissolved pool to the particulate pool per day (Eqs. 3 and 4, respectively):

$$\begin{aligned} & \text{Cd}_{\text{total}} \text{Uptake Rate} \left(\text{pmolL}^{-1} \text{d}^{-1} \right) \\ &= \frac{\left[^{110}\text{Cd}_{\text{Sample}} \left(\text{pmolL}^{-1} \text{d}^{-1} \right) - ^{110}\text{Cd}_{\text{PEP}} \left(\text{pmolL}^{-1} \text{d}^{-1} \right) \right]}{\left[^{110}\text{Cd}_{\text{Spike}} \left(\text{pmolL}^{-1} \right) + ^{110}\text{Cd}_{\text{Natural}} \left(\text{pmolL}^{-1} \right) \right]} \\ & \times \text{Cd}_{\text{total}} \left(\text{pmolL}^{-1} \right) \end{aligned} \quad (3)$$

$$\begin{aligned} & \text{Zn}_{\text{total}} \text{Uptake Rate} \left(\text{pmolL}^{-1} \text{d}^{-1} \right) \\ &= \frac{\left[^{67}\text{Zn}_{\text{Sample}} \left(\text{pmolL}^{-1} \text{d}^{-1} \right) - ^{67}\text{Zn}_{\text{PEP}} \left(\text{pmolL}^{-1} \text{d}^{-1} \right) \right]}{\left[^{67}\text{Zn}_{\text{Spike}} \left(\text{pmolL}^{-1} \right) + ^{67}\text{Zn}_{\text{Natural}} \left(\text{pmolL}^{-1} \right) \right]} \\ & \times \text{Zn}_{\text{total}} \left(\text{pmolL}^{-1} \right) \end{aligned} \quad (4)$$

2.9 Nutrient analyses

Seawater samples taken for macronutrient analysis were filtered through 0.2 μm Supor (Pall) membrane filters and frozen at sea in acid-washed 60 mL high-density polyethylene (HDPE) bottles until analysis. Nutrient analyses were conducted by nutrient autoanalyzer by Joe Jennings at Oregon State University using previously described methods (Noble et al., 2012).

2.10 Statistics and plotting

Dissolved ecological stoichiometries were obtained from the slopes of two-way (type II) least-squares linear regressions performed using the script `lsqfitma.m` rewritten from MATLAB to Python by Rebecca Chmiel (<https://github.com/rebecca-chmiel/GP15>, last access: 14 December 2024). A correlation matrix of various parameters measured dur-

ing NBP18-01 was created with SciPy v1.5.2 using the “`scipy.stats.pearsonr`” function, yielding Pearson correlation coefficients and p values that were visually represented using Seaborn v0.11.1 and Matplotlib v3.3.2. Ocean sections were plotted using Ocean Data View v5.3.0 with gridded bathymetry file ETOPO1_2min. Outliers (see the “Data availability” section at the end of the paper) were excluded from ocean sectional plots. Mixed-layer depth was calculated using the potential density function (ρ_{den}) within the python-seawater module (v3.3.4). Depth-integrated uptake rates were calculated using the “`auc`” function within the scikit-learn (v0.23.2) Python library. Figures were made using Matplotlib (v3.3.2), Ocean Data View (v5.5.2), Excel (2019), and RStudio (v1.3.1093). Ocean Data Viewer color palettes (<https://doi.org/10.5281/zenodo.1243862>) are inverse “roma” for trace metal and macronutrient concentrations, “thermal” for Zn and Cd uptake rates, and “algae” for total fluorescence (Cramer, 2023).

3 Results

3.1 Amundsen Sea

Zn and Cd uptake rate experiments were conducted at 18 stations. We define 3 groups of stations based on location: the Amundsen Sea, Ross Sea, and Terra Nova Bay (TNB) groups (Fig. 1). Uptake rates were assessed at three stations (4, 11, and 15) within the Amundsen Sea group, six stations (20, 29, 32, 35, 62, and 67) within the Ross Sea group, and nine stations (22, 27, 41, 46, 52, 57, 72, 76 and 79) within the TNB group, spanning ~ 10 –250 m depth for a total of 18 stations and 125 samples. An overall schematic detailing these experiment workflows is shown in Fig. 2. The experimental design was validated by comparison of surface particulate ^{67}Zn : ^{68}Zn and ^{110}Cd : ^{114}Cd ratios measured in spiked samples with natural abundance ratios. Samples spiked with ^{67}Zn had particulate ^{67}Zn : ^{68}Zn ratios larger than natural abundance ratios at all stations (as was also true for ^{110}Cd spiked samples and Cd natural abundances; Fig. S1), indicative of uptake of the spike into the particulate phase.

The Amundsen Sea stations represented a linear cruise track, and we report total dissolved metal concentrations (dMetal_{T}) and uptake rates (ρ_{Metal}) over time in order of station sampling date (Fig. 3a). Among these stations, total Chl fluorescence was lowest at station 4 and increased moving westward along the transect to a Chl maximum of 41.8 mg m^{-3} at station 15, 10 m (Fig. 3b). Maximum surface concentrations of dZn, dCd, and dMn were highest at station 4 (3.5 nM, 639 pM, and 2.6 nM at 10 m, respectively; Fig. 3e, f, h), likely reflecting the relatively small amount of total biomass (as indicated by total Chl fluorescence; Fig. 3b) at this station. Concentrations of dZn, dCd, and dMn decreased moving westward along the transect (Fig. 3e, f, h) as total Chl fluorescence increased (Fig. 3b). Total Zn up-

take rates (ρZn) and total Cd uptake rates (ρCd) were highest at station 11 (158 and 21 $\text{pmol L}^{-1} \text{d}^{-1}$, respectively, at 10 m; Figs. 3c, d; 4b). Among the three Amundsen Sea stations, the largest movement of both Zn and Cd into the particulate phase therefore occurred at station 11, concurrent with the relatively high dFe_T surface values observed at station 11 (0.2 nM dFe compared to 0.01 nM at station 4, 10 m; Figs. 3g, S3c). The dFe concentrations exceeding 1 nM near the seafloor are consistent with a sedimentary or subglacial source (Fig. S3c). Overall, ρZn and ρCd profiles exhibited trends in which values were highest within the upper 50 m at all three stations and decreased with depth, following the trend in Chl *a* or total Chl fluorescence (Fig. 4). Vertical sections of dZn and dCd through the water column mirrored these trends (Fig. 4), demonstrating the movement of these dissolved metal micronutrients into the particulate phase.

3.2 Ross Sea

We next investigated the dissolved Zn and Cd demand of the natural phytoplankton community at stations sampled over the Ross Sea shelf. Data collected from this group are presented over time in order of sampling date (Fig. 5). We note that unlike the Amundsen Sea sector, the stations sampled in this group did not follow a linear cruise track, and thus we cannot make inferences regarding latitudinal or longitudinal changes. Surface Chl fluorescence was highest at stations 32 and 67 with maximum values of 15.8 and 14.6 mg m^{-3} at 25 and 10 m, respectively (Fig. 5b). With the exception of station 20, dZn and dCd demonstrated high levels of surface depletion within the upper 25 m (Fig. 5e, f), with average concentrations of 0.63 ± 0.13 and 0.19 ± 0.09 nM, respectively, at ≤ 10 m. Compared to 100 m values (i.e., below the MLD), concentrations at 25 m were equivalent to 87 %, 34 %, 85 %, 85 %, 77 %, and 88 % decreases in dZn and 83 %, 19 %, 84 %, 67 %, 64 %, and 75 % decreases in dCd at stations 32, 20, 67, 35, 29, and 62, respectively. Measured dMn concentrations were also highly depleted within the upper 250 m at all Ross Sea stations (average 10 m $\text{dMn} = 0.18 \pm 0.26$ nM; Fig. 5h). While dFe was depleted within the upper 10 m at all stations (average dFe concentration at 10 m = 0.12 ± 0.12 nM), concentrations exceeding 1 nM were observed below 100 m at station 32 (Fig. 5g) and extended down to 650 m (Fig. S4c), implying a sedimentary source. The largest Zn uptake rate measured among all stations in this group (115 $\text{pmol L}^{-1} \text{d}^{-1}$) was observed at station 32 at 10 m (Fig. 6c). As observed in the Amundsen Sea, ρZn , ρCd , and total Chl *a* or Chl fluorescence profiles exhibited surface maxima and became depleted with depth and were again mirrored by nutrient-like dZn and dCd depth profiles (Fig. 6), indicative of uptake of these metals into the particulate phase in surface waters.

3.3 Terra Nova Bay

Zinc and Cd uptake rate data collected from stations sampled in Terra Nova Bay (TNB) were visualized over time due to repeated sampling within a small geographic region and similar time frame (Fig. 7a). This allowed for an analysis of how dissolved metal concentrations and metal uptake rates changed throughout January–February 2018 within the same spatial area. Station data are presented in order of sampling date from earliest (station 22, sampled in early January) to latest (station 79, sampled in late February).

Surface Chl fluorescence was highest in early January ($\sim 18 \text{ mg m}^{-3}$) and waned into February (Fig. 7b), similar to observed trends in Zn and Cd uptake rates (Fig. 7c, d). Of all TNB stations, stations 22 and 27, sampled in January, had the highest maximum Zn uptake rates of 89.9 and 46.0 $\text{pmol L}^{-1} \text{d}^{-1}$, respectively, at 10 m (Fig. 8a, b). Cd uptake rates were also highest at these stations with values of 13.4 and 20.1 $\text{pmol L}^{-1} \text{d}^{-1}$ (Fig. 8a, b). At the final station (station 79, sampled in late February), maximum uptake rates of both metals had sharply decreased to 24.7 and 5.0 $\text{pmol Zn L}^{-1} \text{d}^{-1}$ (Fig. 8i). Overall, maximum uptake rates of both metals decreased over time within TNB (Fig. 7c, d), consistent with the decrease in total Chl fluorescence (Fig. 7b), likely due to the aging of and decline in the phytoplankton bloom.

Surface depletion of dZn , dCd , and dMn was observed at all stations, with average dissolved concentrations of 0.82 ± 0.47 nM Zn, 0.13 ± 0.06 nM Cd, and 0.08 ± 0.04 nM Mn at 10 m depth (Fig. 7e, f, h). Notably, increased surface concentrations of dZn , dCd , and dMn were apparent at the late stations 72, 76, 78, and 79, with $\text{dZn} \sim 2$ nM, $\text{dCd} \sim 300$ pM, and $\text{dMn} \sim 0.2$ nM (Fig. 7e, f, h; Fig. S5). Dissolved macronutrient (phosphate, nitrate and nitrite, and silicate) concentrations also followed this trend, with increased surface concentrations at the late stations (Fig. S6). As with the Amundsen and Ross Sea station groups, Zn and Cd uptake rates within TNB tended to be highest at the surface ≤ 50 m as also observed in total Chl fluorescence trends, and this mirrored the decrease in total dissolved Zn and Cd (Fig. 8). Unlike the Amundsen and Ross Sea stations, where Cd uptake consistently became negligible ($\sim 0 \text{ pM L}^{-1} \text{d}^{-1}$) by 100 m (Figs. 4; 6), measurable Cd uptake persisted in TNB to 150 m at stations 72 and 79 (Fig. 8g, i). Measurable Zn uptake rates were also captured at deeper depths at these late TNB stations (Fig. 8g, h, i).

The increased surface concentrations of dZn and dCd and macronutrients, as well as the persistence of measurable uptake rates at deeper depths, at these late TNB stations may be attributed to the deepening of the mixed layer (Fig. S7). Vertical mixing was evidenced by more uniform potential densities, temperatures, dissolved oxygen (O_2) concentrations, salinity, and beam transmission measurements at the late TNB stations within the upper 200 m (Fig. S7). Higher (> 0.5 nM) dFe concentrations were also observed below

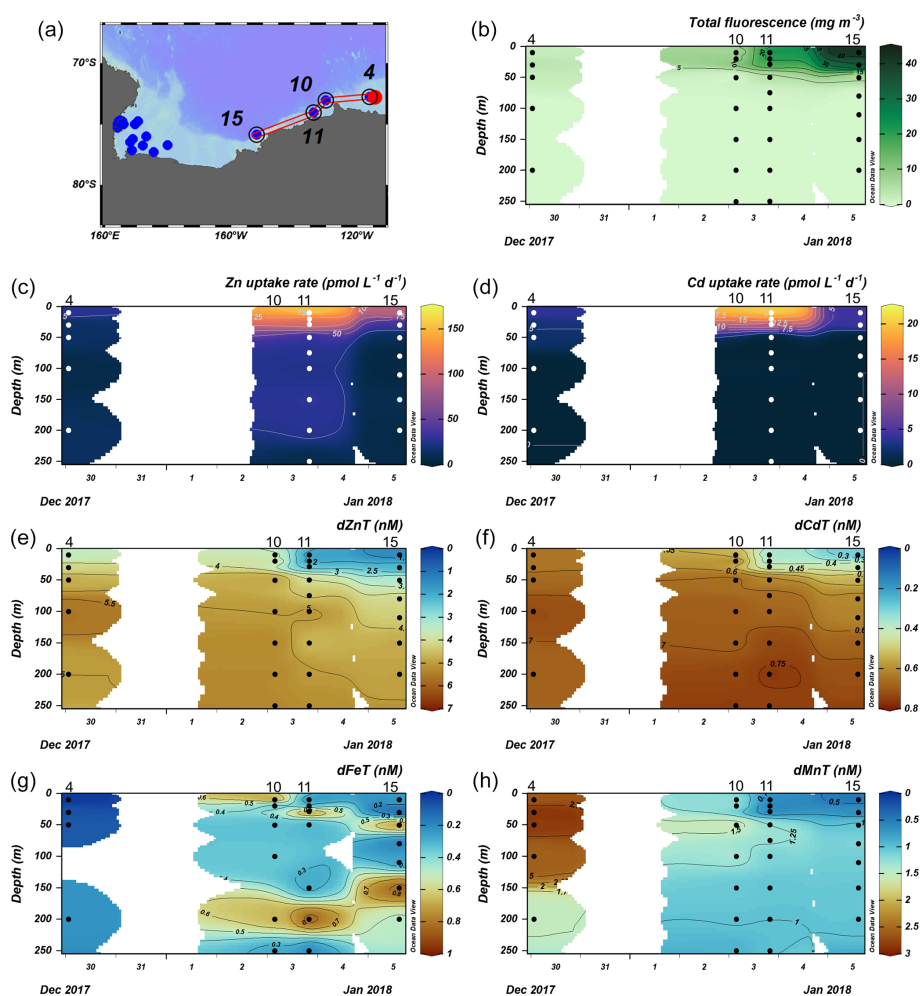


Figure 3. Total fluorescence and trace metal concentrations measured at Amundsen Sea stations shown over time. (a) Map showing station locations, (b) total chlorophyll (Chl) fluorescence, (c) total Zn uptake rates, (d) total Cd uptake rates, (e) total dissolved Zn, (f) total dissolved Cd, (g) total dissolved Fe, and (h) total dissolved Mn measured in the upper 250 m represented on a color scale. Uptake experiments were not performed at station 10. Metal concentrations measured to 500 m depth are shown in Fig. S3. The following abbreviations are used: dZnT is total dissolved Zn, dCdT is total dissolved Cd, dFeT is total dissolved Fe, and dMnT is total dissolved Mn.

100 m at these late stations (Fig. 7g) and increased with depth (> 2 nM), as did dZn and dMn concentrations, possibly due to sedimentary inputs (Giordano et al., 1999) (Fig. S5). At these late stations (station 76, 78, 79) mixing replenished surface concentrations of both macronutrients (Fig. S6) and dZn (Fig. S5a), but dZn was replenished to a lower extent. For example, comparing 50 m “replenished” surface values of P, N+N, and Si to deepwater (200 m) values at station 79, percent changes from deep to surface values were -0.35% for P, -0.30% for N+N, and -0.26% for Si (where a percent change of 0 would indicate complete replenishment; i.e., if nutrient values at 200 and 50 m were equal). In contrast, the percent change from deep (200 m) to surface (50 m) dZn at station 79 was lower at -0.71% . Hence, dZn was apparently replenished to a lesser extent compared to macronutrients, which may reflect a sustained high demand for Zn generating

a dearth of this micronutrient despite macronutrient replenishment.

3.4 Overview of Zn and Cd uptake at 18 stations

We next summarize the maximum Zn and Cd uptake rates observed at each station (all of which were observed at ≤ 10 m depth; Fig. 9a, b) with uptake rates normalized to Chl *a* ($\mu\text{g L}^{-1}$) as a proxy for biomass (Fig. 9c, d). Overall, high (> 25 $\text{pmol L}^{-1} \text{d}^{-1} \text{Chl } a$ ($\mu\text{g L}^{-1}$) $^{-1}$) Chl *a*-normalized Zn uptake rates were measured at station 11 in the Amundsen Sea and at stations 20 and 32 in the Ross Sea (Fig. 9c). The highest Chl *a*-normalized Cd uptake rates among all 18 stations were also measured at stations 20 and 32 (Fig. 9d). Across TNB, Chl *a*-normalized maximum Zn and Cd uptake ranged from 6.0–28.3 $\text{pmol L}^{-1} \text{d}^{-1} \text{Chl } a^{-1}$ for Zn and 3.4–9.3 $\text{pmol L}^{-1} \text{d}^{-1} \text{Chl } a^{-1}$ for Cd (Fig. 9c, d). Integrated

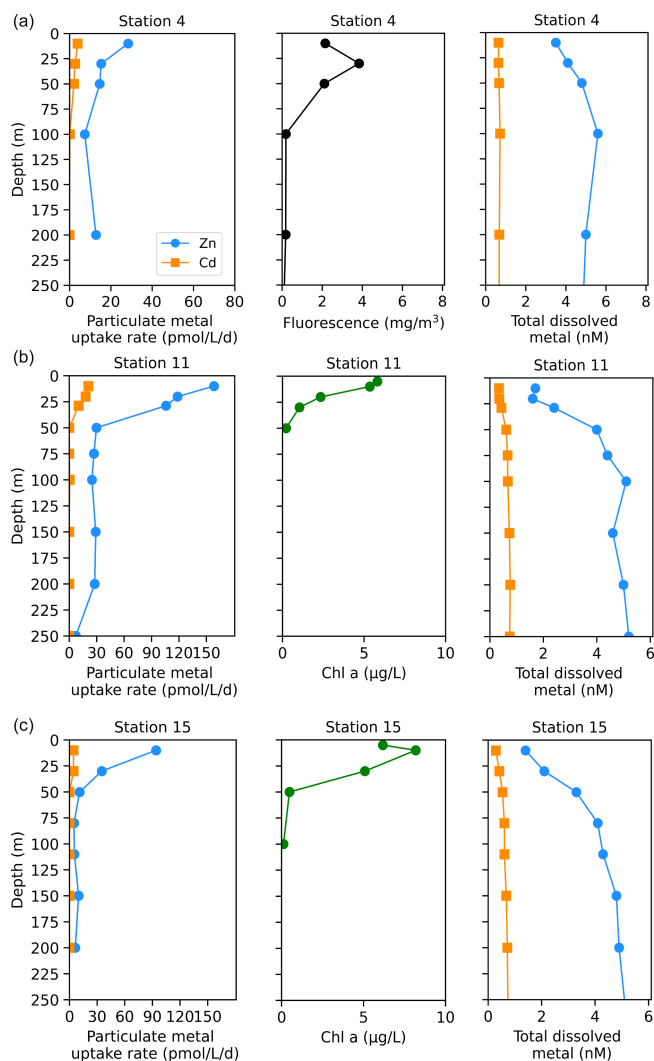


Figure 4. Depth profiles of total Zn and Cd uptake rates, total chlorophyll fluorescence (or chlorophyll *a*), and total dissolved metal measured in the upper 250 m at (a) station 4, (b) station 11, and (c) station 15 sampled along the Amundsen Sea shelf. Total chlorophyll (Chl) fluorescence is reported for stations where chlorophyll *a* (Chl *a*) data were not measured.

(10–250 m) uptake rate values were highest for Zn at stations 11 and 32 and highest for Cd at station 32 (Fig. 9e, f). Increases in integrated Cd and Zn uptake at the late stations 72, 76, and 79 reflected the deeper depths to which uptake rates of these metals remained measurable, likely reflecting deepened mixed layers (Fig. S7) and/or sinking of the phytoplankton community, as seen in the fluorescence data to beyond 150 m depth (Fig. 7b). The presence of Chl *a* (Fig. 8g, i) implies these deep phytoplankton communities may have been alive if not actively photosynthesizing. We previously identified ZCRP-B, a membrane-associated protein involved in high-affinity Zn transport (Kellogg et al., 2022). These proteins have a single transmembrane domain, implying func-

tion as a membrane-tethered ligand to assist in the acquisition of Zn from seawater in cooperation with adjacent zinc transporters (ZIP transporters). Hence, ZCRP-B could be a potential site of Zn binding and “uptake”, as our uptake rate measurements do not discern between extracellular and intracellular Zn, even if the phytoplankton are inactive due to a lack of photosynthetic energy at these depths.

Notably, maximum Cd uptake rates measured in the present study were 3.4, 3.7, and 3.3 times higher in the Amundsen Sea, Ross Sea, and Terra Nova Bay, respectively, compared to the maximum Cd uptake rate of $6.1 \text{ pmol L}^{-1} \text{ d}^{-1}$ measured previously within the Costa Rica Dome using identical methods (Cox et al., 2014), demonstrating the influence of high productivity and the native community on the flux of dCd into the particulate phase.

4 Discussion

4.1 Use of metal uptake rates to determine depletion time frames

The measurement of total dissolved metal concentrations over large latitudinal or longitudinal areas allows for the characterization of metal inventories, though these are snapshots of inventories observed at specific times. The measurement of metal uptake rates allows us to gain new insight into how these inventories came to be and the time frames over which they are consumed and replenished. Due to the resetting of surface dissolved metal concentrations to those of deepwater values during austral winter with deep winter mixing, the Ross Sea of the Southern Ocean is particularly applicable to this type of time frame study (Sedwick and DiTullio, 1997; Sedwick et al., 2011).

Using the Zn uptake rates measured in this study, we can estimate the time required for the high levels of primary production observed in the Southern Ocean to draw down surface dZn from high (deep-water) winter concentrations to the surface concentrations observed during austral summer 2017. The Southern Ocean growing season typically spans October–March, with primary productivity peaking November–January and the area of open (ice-free) water over the Ross Sea shelf linearly increasing from November to mid-January (Sedwick et al., 2011). Vertical profiles of nutrients and micronutrients in coastal Antarctic ecosystems such as the Ross Sea are reset and become uniform with depth during the winter months due to whole water column mixing and an absence of photosynthetic activity during the dark winter under the sea ice (Noble et al., 2013). As a result, the draw-down of nutrients in the upper water column observed during the spring and summer seasons is the result of less than 1 year’s biological influence. For this simple calculation, we ignore the upward flux of Zn (upwelling = 0) and assume a high export ratio of 0.8 due to bloom productivity being dominated by diatoms and *Phaeocystis antarctica*, both of which

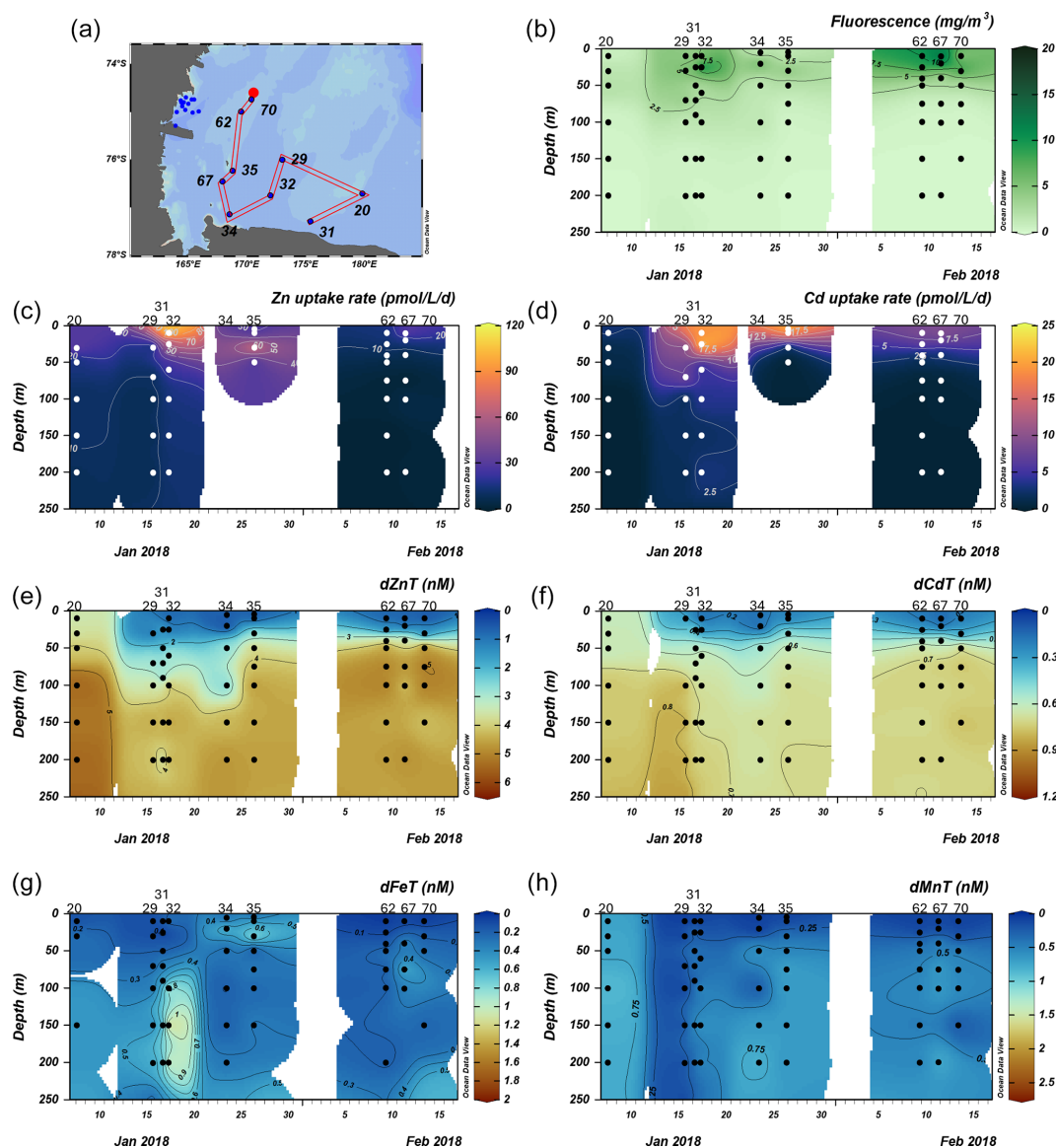


Figure 5. Total fluorescence and trace metal concentrations measured at Ross Sea stations shown over time. (a) Map showing station locations, (b) total chlorophyll (Chl) fluorescence, (c) total Zn uptake rates, (d) total Cd uptake rates, (e) total dissolved Zn, (f) total dissolved Cd, (g) total dissolved Fe, and (h) total dissolved Mn measured in the upper 250 m represented on a color scale. Uptake experiments were not performed at stations 31, 34, and 70. Metal concentrations measured to 800 m depth are shown in Fig. S4. The following abbreviations are used: dZnT is total dissolved Zn, dCdT is total dissolved Cd, dFeT is total dissolved Fe, and dMnT is total dissolved Mn.

sink rapidly and thus contribute substantially to carbon export flux (Asper and Smith, 1999; DiTullio et al., 2000). The depletion of dZn from a surface box was therefore estimated as follows:

$$\left(\frac{dZn}{dt}\right)_{\text{surface box}} = -\rho Zn + (Rf \times \rho Zn) + \text{upwelling},$$

where Rf is the remineralization factor equal to $1 - \text{export ratio}$.

When taking station 11, for which the highest Zn uptake rate was observed, as an extreme case, with a maximum Zn

uptake rate of $158 \text{ pmol L}^{-1} \text{ d}^{-1}$, it would take only 25 d to deplete a surface winter concentration of 4.8 nM (i.e., the average deepwater ($< 200 \text{ m}$) dZn concentration for all stations measured in this study) down to the observed surface concentration of 1.7 nM at station 11 (Fig. 4b), assuming a constant uptake rate and no additional inputs of dissolved Zn (Fig. 10).

Given that dZn surface depletion to sub-nanomolar levels was observed throughout much of the CICLOPS expedition, prolonged high levels of Zn uptake and export that overwhelm replenishment by vertical mixing and/or remineralization are likely key to giving rise to the observed ex-

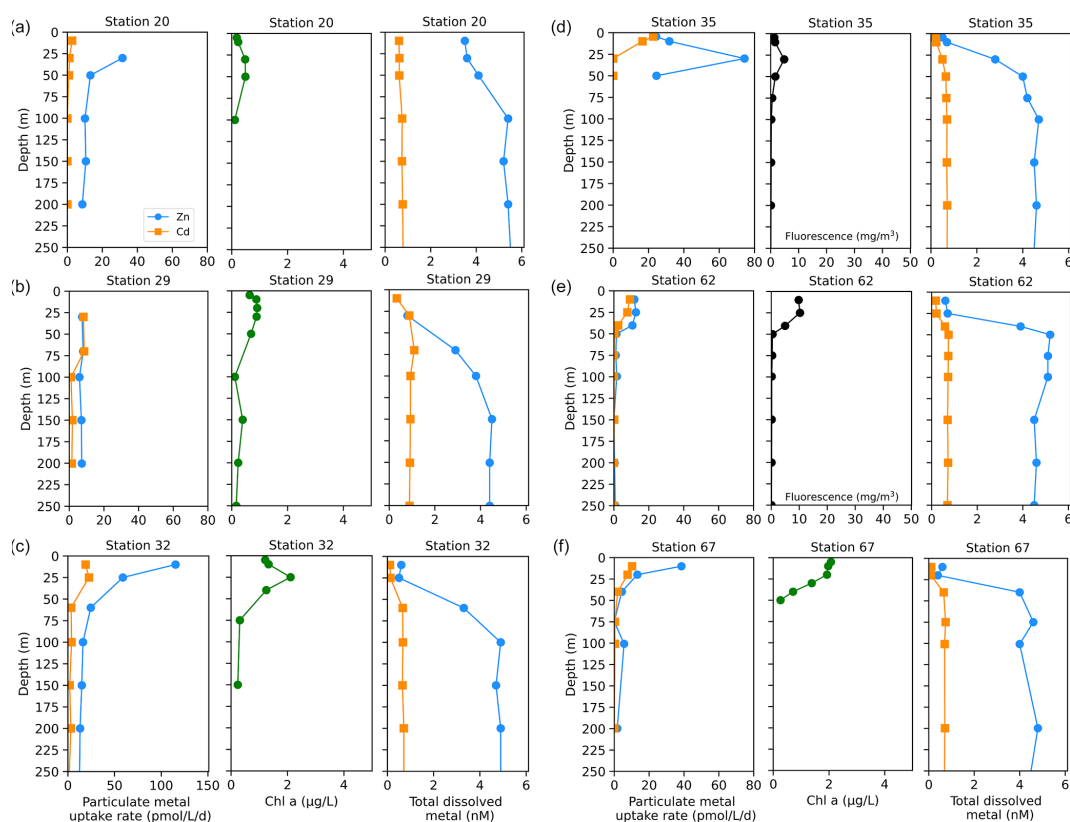


Figure 6. Depth profiles of total Zn and Cd uptake rates, total chlorophyll fluorescence (or, where available, chlorophyll *a*), and total dissolved metal ($dMetal_T$) measured in the upper 250 m at (a) station 20, (b) station 29, (c) station 32, (d) station 35, (e) station 62, and (f) station 67 sampled along the Ross Sea shelf. Total chlorophyll (Chl) fluorescence is reported for stations where chlorophyll *a* (Chl *a*) data were not measured.

tent of seasonal surface dZn depletion. These calculations were conducted as a proof-of-concept demonstration to determine if uptake rates were sufficient to draw down the otherwise abundant dZn inventory on seasonal timescales. An important caveat to this calculation is that the regulation and production of Zn sensors that modulate Zn uptake, export, and storage will naturally fluctuate in response to changing dZn and therefore cannot be assumed to be constant. Future studies could conduct mesoscale modeling of the region, including eddy diffusion and advection. Notably, any dZn upwelling flux into the euphotic zone would require even higher Zn uptake rates to create the seasonal surface Zn depletion we observed on this expedition.

4.2 Influences on Zn and Cd uptake

We next consider the factors driving the magnitude of ρZn and ρCd . As noted above, ρZn and ρCd were positively correlated with total Chl fluorescence or Chl *a* at every station (Figs. 4, 6, and 8), demonstrating the influence of total autotrophic biomass on uptake rates. A Pearson correlation analysis comparing the abundance of individual algal pigments to ρZn and ρCd throughout the water column for all

stations revealed significant, positive correlations (Pearson correlation coefficient > 0.50 , $p \leq 1.2 \times 10^{-4}$) between ρZn and Chl *a*; Chl *b*; and Chl *c*1, *c*2, and *c*3. Pearson correlation coefficients are normally symbolized as rho (ρ), but they are herein referred to as “PCC” values to avoid confusion with our uptake rate symbol (ρ) and p values (p). The correlation between ρZn and Chl *b* was the strongest (PCC = 0.77, $p = 3.8 \times 10^{-10}$) of any pigment (Fig. 11e).

In bottle incubation experiments conducted at station 27, the addition of Zn alone resulted in the positive growth response of algae containing Chl *b* (small green algae such as prasinophytes; Kell et al., 2023), corroborating this finding. ρCd also positively correlated with these Chl pigments but with slightly lower Pearson correlation coefficients (PCC = 0.3–0.51, $p \leq 4.3 \times 10^{-2}$). Fucoxanthin (fuco) concentrations were more highly correlated with ρCd (PCC = 0.57, $p = 4.3 \times 10^{-5}$) than with ρZn (PCC = 0.32, $p = 2.9 \times 10^{-2}$), while the opposite was observed for 19'-Hex (19'-hexanoyloxyfucoxanthin; PCC = 0.54, $p = 1.1 \times 10^{-4}$ for Zn; not significant for Cd) (Fig. 11e). Fuco and 19'-Hex are used as taxonomic indicators of diatoms and *Phaeocystis*, respectively, in the Ross Sea (DiTullio et al., 2003, 2007; DiTullio and Smith, 1995; Wright et al., 2010). The

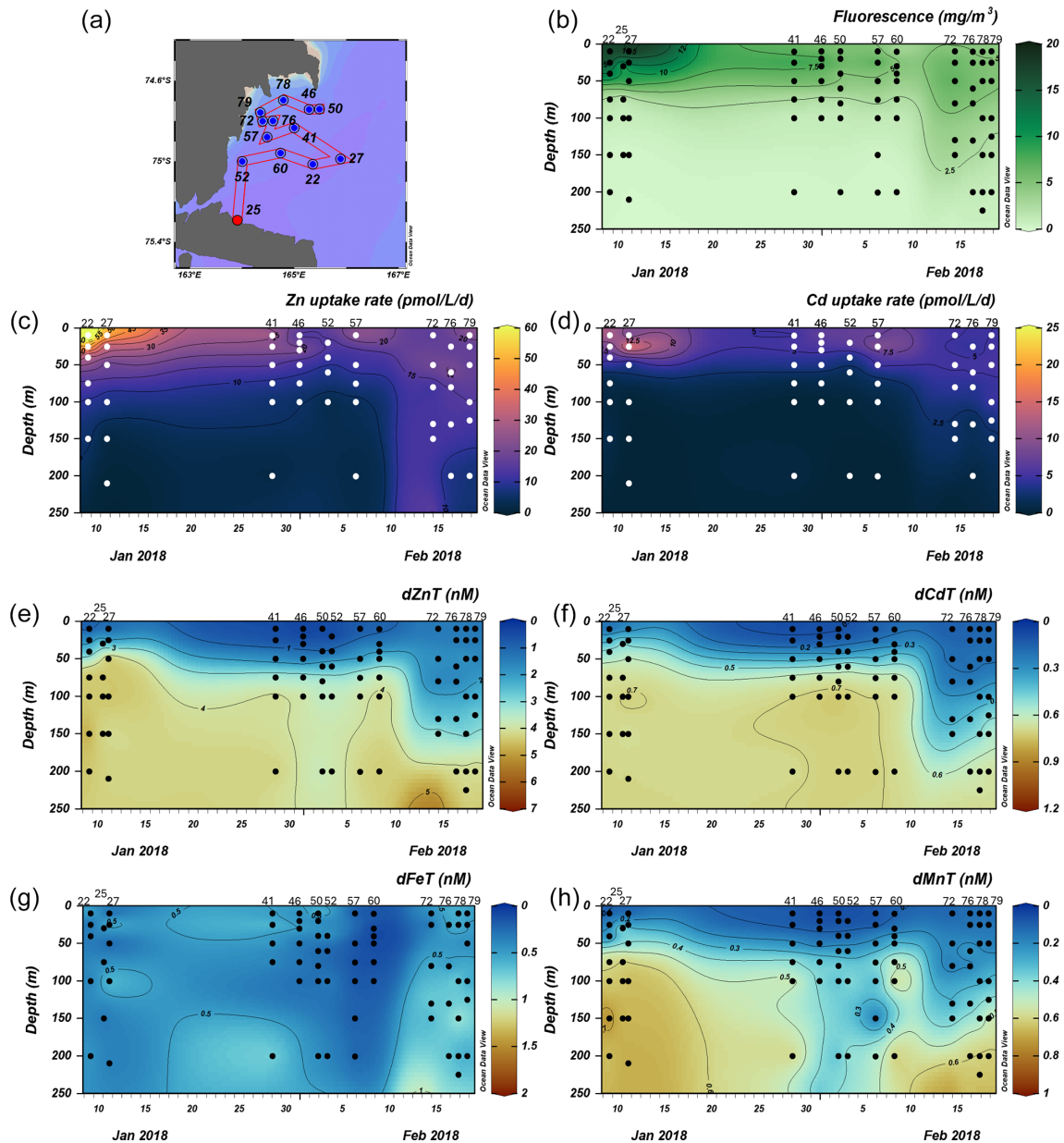


Figure 7. Total fluorescence and trace metal concentrations measured at Terra Nova Bay (TNB) stations shown over time. (a) Map showing station locations, (b) total chlorophyll (Chl) fluorescence, (c) total Zn uptake rates, (d) total Cd uptake rates, (e) total dissolved Zn, (f) total dissolved Cd, (g) total dissolved Fe, and (h) total dissolved Mn measured in the upper 250 m represented on a color scale. Uptake experiments were not performed at stations 70 and 34. Metal concentrations measured to 600 m depth are shown in Fig. S5. The following abbreviations are used: dZnT is total dissolved Zn, dCdT is total dissolved Cd, dFeT is total dissolved Fe, and dMnT is total dissolved Mn.

higher correlation coefficient between ρZn and *Phaeocystis* abundance (as indicated by 19'-Hex) implies that Zn uptake was driven largely by *Phaeocystis*. This finding is consistent with the detection of *Phaeocystis* ZCRP-A, a protein characterized as an algal Zn²⁺ metallochaperone (Kellogg et al., 2022), in metaproteomic data collected from both the incubation experiment and throughout the water column at station 27 (Kell et al., 2023). The positive correlation between ρCd and the abundance of diatoms (as indicated by

fuco) is consistent with the diatomic utilization of Cd as a nutrient within CDCA metalloenzymes, as *cdca* genes have, to date, been found exclusively in diatom species (Park et al., 2007, 2008). While it is likely that both *Phaeocystis* and diatoms contributed to the Cd and Zn uptake rates measured here, it is currently unknown if *Phaeocystis* can utilize Cd as a nutrient. Overall, any potential growth benefit conferred by our Cd spike additions may only have been applicable to diatoms that (1) possessed the *cdca* gene and (2) faced selec-

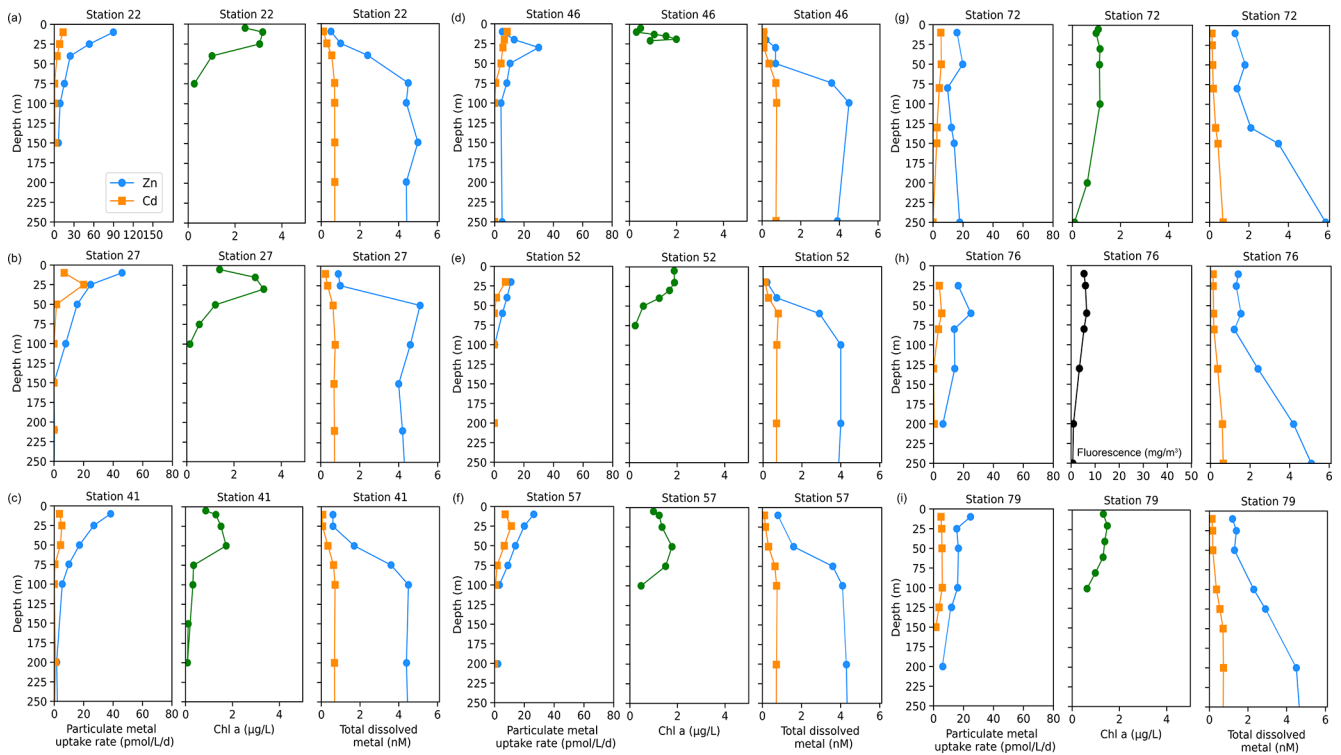


Figure 8. Depth profiles of total Zn and Cd uptake rates, total chlorophyll fluorescence (or, where available, chlorophyll *a*), and total dissolved metal (dMetalT) measured in the upper 250 m at (a) station 22, (b) station 27, (c) station 41, (d) station 46, (e) station 52, (f) station 57, (g) station 72, (h) station 76, and (i) station 79 within Terra Nova Bay. Total chlorophyll (Chl) fluorescence is reported for stations where chlorophyll *a* (Chl *a*) data were not measured.

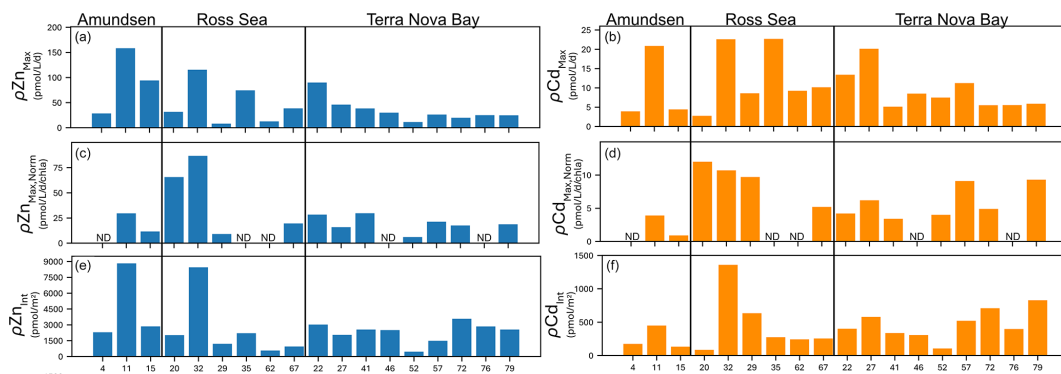


Figure 9. Unnormalized (a) maximum Zn uptake rates ($\rho\text{Zn}_{\text{Max}}$) and (b) maximum Cd uptake rates ($\rho\text{Cd}_{\text{Max}}$) at each station grouped by area (Amundsen Sea, Ross Sea, Terra Nova Bay). (c) $\rho\text{Zn}_{\text{Max}}$ and (d) $\rho\text{Cd}_{\text{Max}}$ normalized to chlorophyll *a* ($\mu\text{g L}^{-1}$) measured at each station. (e) Depth-integrated (10–250 m) ρZn and (f) ρCd values at each station. ND indicates no data (chlorophyll *a* not measured).

tion pressure to utilize Cd as a cofactor in CDCA due to low seawater pCO_2 (as documented on this expedition), creating enhanced demand for dZn. The presence of Cd-utilizing diatoms in the water column at station 27 was demonstrated by the detection of CDCA transcripts with closest taxonomic matches to the diatom genera *Chaetoceros* and *Corethron* (Kell et al., 2023). Station 27 also exhibited high surface Chl fluorescence (19.3 mg m^{-3} at 10 m), low pCO_2 ($221 \mu\text{atm}$ at

5 m), and high maximum Zn and Cd uptake rates (46 and $20 \text{ pmol L}^{-1} \text{ d}^{-1}$, respectively), demonstrating a high algal demand for Zn that likely created pressure for Cd uptake.

We next consider the effect of the depleted seawater pCO_2 levels induced by the high biomass conditions observed on this expedition. Previously, a strong correlation between dissolved $\delta^{114}\text{Cd}$ and dissolved CO_2 was documented in the Atlantic sector of the Southern Ocean (de Baar et al., 2017),

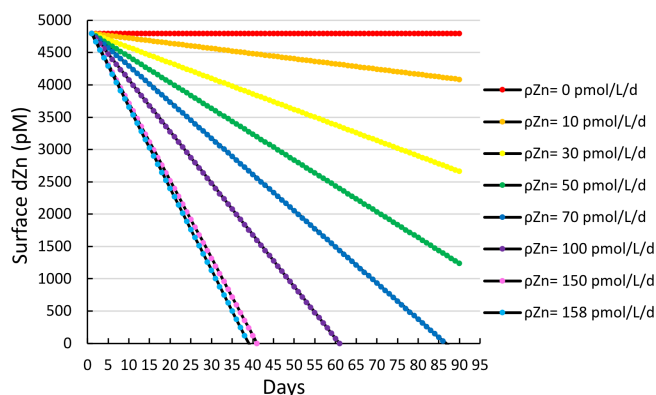


Figure 10. A simple model estimating the time (in days) required to deplete the estimated average winter surface concentration of dZn (4.8 nM) over a range of various Zn uptake rates (ρZn). A value of $158 \text{ pmol L}^{-1} \text{ d}^{-1}$ was the maximum Zn uptake rate observed in this study (station 11, 10 m).

suggesting significant Cd isotope fractionation due to biological uptake into the particulate phase. A relationship between total surface Cd uptake rates at 10 m and surface pCO_2 (underway, measured at 5 m) was not observed in the present study (Fig. 11b). The present study includes measurements of total Cd uptake (i.e., the sum of all Cd isotopes) using an added Cd isotope tracer, and hence we did not explore natural isotope fractionation effects. However, we did observe a significant negative linear relationship between total Zn uptake rates and seawater pCO_2 ($m = -0.58$, $R^2 = 0.63$; Fig. 11a) consistent with an increased demand for Zn^{2+} to power the carbon-concentrating mechanism of photosynthetic algae under lower CO_2 availability. ρZn and ρCd furthermore shared a significant positive linear relationship with each other ($m = 0.13$, $R^2 = 0.64$; Fig. 11c) (as was also reflected in the Pearson correlation test; $\text{PCC} = 0.69$, $p = 1.7 \times 10^{-7}$, Fig. 11d) implying that as demand for Zn increased, demand for Cd also increased, consistent with laboratory studies showing their co-transport in marine algae (Sunda and Huntsman, 2000). We also note that $\rho\text{Cd} : \rho\text{Zn}$ uptake ratios were higher (> 0.4) at the surface where total dissolved $\text{dCd} : \text{dZn}$ ratios were comparatively high (> 0.3) (Fig. S8a, b). The strong positive linear relationship shared between these ratios ($R^2 = 0.82$; Fig. S8c) further suggests that dZn levels were depleted enough to induce increased Cd uptake rates and is consistent with their known biochemical substitution within marine algae.

Algal Cd uptake rates are known to be inversely related to both Mn^{2+} and Zn^{2+} concentrations in cultures (Lee et al., 1995; Sunda and Huntsman, 1996), which is thought to reflect the uptake of Cd by two separate inducible transport systems. Cd is taken up competitively by the high-affinity Zn uptake system under low Zn^{2+} conditions, as demonstrated above, while Cd, Zn, and Mn share the same low-affinity Mn uptake system under high Zn^{2+} conditions (Lee

et al., 1995; Sunda and Huntsman, 1998b, a, 2000; Xu et al., 2007). With the exception of the Amundsen Sea stations, dMn was consistently observed at concentrations of only 0.1–0.5 nM within the upper 50 m (Figs. 3h; 5h; 7h). Low surface dMn concentrations within the Southern Ocean have been documented previously and were attributed to a combination of biological uptake at the surface causing depletion and low resupply due to few external sources (Lattour et al., 2021). While ρCd was negatively correlated with dMn ($\text{PCC} = -0.34$, $p = 0.02$) considering all stations and all depths, ρCd was more strongly negatively correlated with dZn ($\text{PCC} = -0.76$, $p = 1.1 \times 10^{-9}$), which was the strongest negative correlation when comparing all measured parameters to ρCd (Fig. 11d). This finding is consistent with decreased dCd uptake where dZn availability is sufficient. Overall, these results are consistent with biology (total biomass) and pCO_2 acting as primary influences on ρZn , with increases in ρZn leading to increases in ρCd through the upregulation of a shared transport system.

4.3 Effects on dCo cycling

In addition to Cd, the intense Zn demand captured by these uptake rates also appears to have shifted the demand for the trace metal micronutrient cobalt (Co) (Chmiel et al., 2023). Due to their similar charge and atomic radii, Zn^{2+} , Co^{2+} , and Cd^{2+} cations often share the same transporter uptake systems. An organism's ability to utilize these metals as metabolic cofactors is influenced by their environment and the affinity of the uptake ligands for each metal cation (Irving and Williams, 1953; Sunda and Huntsman, 1992). When dZn availability is low, more dCd and dCo are able to bind transport ligands. Therefore, dZn concentrations and cycling can influence the cycling of dCd and dCo, particularly in low dZn environments, as documented for dCd in the present study. The influence of dZn cycling on dCo distributions in this region was also documented during this expedition, with evidence for high rates of biological Co uptake in the Ross Sea driven by dZn (and vitamin B_{12}) scarcity (Chmiel et al., 2023). The high Zn uptake rates measured in this study therefore also reveal dynamic changes in the cycling of Cd and Co as a consequence of high Zn demand.

4.4 The dZn and dCd relationships with macronutrients

The growth of phytoplankton and bacteria in the shallow euphotic zone results in the removal of bioactive trace metals and macronutrients from the dissolved phase into the particulate phase, resulting in dissolved-metal–macronutrient relationships that reflect their collective stoichiometry (Horner et al., 2021). Positive linear slope results generally indicate the co-cycling of the metal and the macronutrient via uptake and remineralization, though slope values can vary widely by basin as they are a function of the metal–macronutrient up-

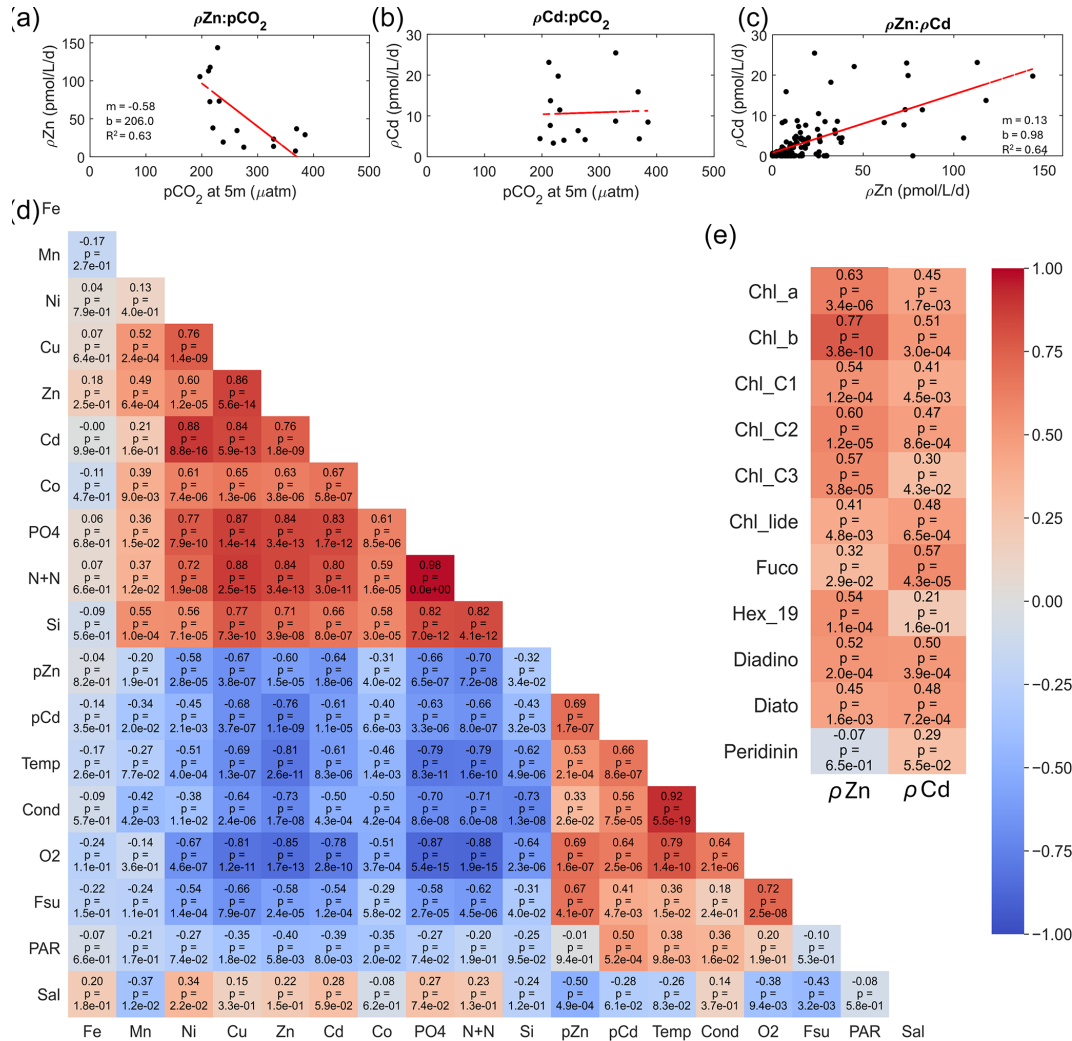


Figure 11. Relationships comparing seawater CO_2 partial pressure (pCO_2) at 5 m depth to (a) Zn uptake rates (ρZn ; $n = 15$, $R^2 = 0.63$) and (b) Cd uptake rates (ρCd ; $n = 15$) measured at surface (≤ 10 m) depths. (c) Relationship between ρZn and ρCd for all depths ($n = 121$, $R^2 = 0.64$). (d) Visual representation of the correlation matrix comparing all water column parameters measured with depth with warm and cool colors indicative of positive and inverse correlations, respectively. Pearson correlation coefficients and p values are shown. (e) Representation of the correlation matrix comparing ρZn and ρCd to various phytoplankton pigments. Fe, Mn, Ni, Cu, Zn, Cd, and Co labels correspond to total dissolved metal concentrations. PO_4 , N+N, and Si correspond to total dissolved concentrations of phosphate, the sum of nitrate+nitrite, and silicate. The following abbreviations are used: Temp is temperature, Cond is conductivity, O_2 is dissolved oxygen, Fsu is total fluorescence, PAR is photosynthetically active radiation, Sal is salinity, Chl_a is chlorophyll a, Chl_b is chlorophyll b, Chl_c1 is chlorophyll c1, Chl_c2 is chlorophyll c2, Chl_c3 is chlorophyll c3, chl_lide is chlorophyllide, Fuco is fucoxanthin, Hex_19 is 19'-hexanoyloxyfucoxanthin, Diadino is diadinoxanthin, and Diato is diatoxanthin.

take and remineralization stoichiometry of the native community and overall nutrient availability. Two-way linear regressions (see Sect. 2.10) were used to investigate the relationships between dZn and dissolved silicate (dSi), dZn and dissolved phosphate (dP), and dCd and dP for the Amundsen Sea, Ross Sea, and TNB station groups (Fig. 12).

The dZn–dP and dCd–dP relationships from this expedition were originally presented in Chmiel et al. (2023) for comparison to dCo :dP, while they are included in the present study for ease of comparison with dZn–dSi relationships

presented for the first time. For these analyses, the depth threshold that separates the surface and deep ocean was manually defined in order to optimize the linear fit of the surface versus deep trends. This threshold depth can be thought of as an inflection point that represents the largest change in trace metal concentration with respect to dP or dSi concentration (Chmiel et al., 2023).

The near-linear global dZn–dSi relationship (Bruland et al., 1978; Middag et al., 2019; Vance et al., 2017) has been posited to arise in part from faster drawdown of Zn and Si

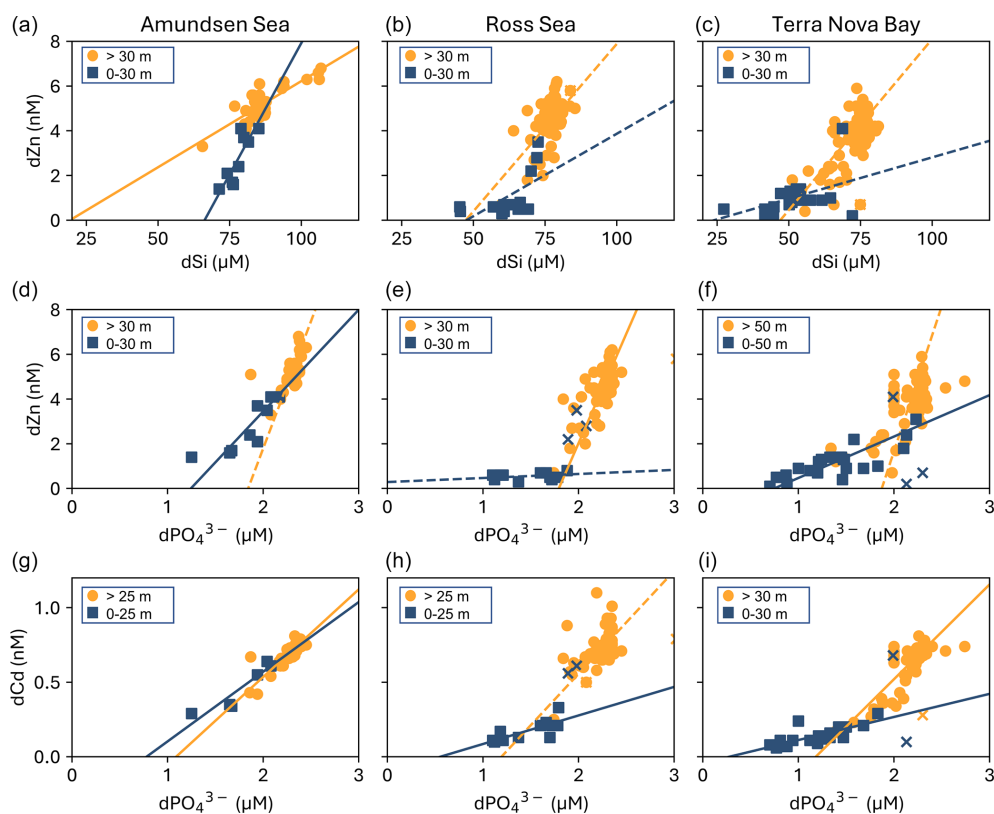


Figure 12. Relationships between (a–c) total dissolved Zn and silicate (dSi), (d–f) total dissolved Zn and phosphate (dPO_4^{3-}), (g–i) and total dissolved Cd and dPO_4^{3-} for the surface (blue squares) and the deep ocean (orange circles) arranged by station group (Amundsen Sea, Ross Sea, and Terra Nova Bay). Depth thresholds were manually chosen to optimize the linear fit of the surface and deep-ocean trends. Regressions with $R^2 \geq 0.50$ are shown as a solid line, and those with $R^2 < 0.50$ are shown as a dotted line. See Table S4 for stoichiometric parameters and values. Regression outliers are marked with “x”. The data used here were originally plotted in Chmiel et al. (2023) and are reprised here for ease of comparison with dZn : Si data.

relative to dPO_4^{3-} into Southern Ocean diatoms that leaves surface waters depleted in Zn and Si (Vance et al., 2017). We observed distinct differences in dissolved dZn : dSi ecological stoichiometries comparing Amundsen Sea, Ross Sea, and Terra Nova Bay station groups (Fig. 12; Table S4). A positive linear dZn–dSi relationship with a steep ($m = 0.23 \pm 0.05$; Table S4) slope observed in the upper ocean of the Amundsen Sea contrasted starkly with the shallow slopes observed in the upper ocean of the Ross Sea and Terra Nova Bay. A bloom of non-silicifying *Phaeocystis antarctica* was present during our passage through the Amundsen Sea, consistent with abundant silicic acid but rapid drawdown of Zn, which is known to be used by this organism (Saito and Goepfert, 2008). In contrast, the shallow slopes in the Ross Sea and Terra Nova Bay resulted from the persistence of dSi concentrations $\geq 30 \mu\text{M}$ in the upper 30 m, while dZn was reduced to sub-nanomolar concentrations (average $\text{dZn} = 0.87 \pm 0.42 \text{ nM}$ in TNB at 10 m depth, $n = 11$), highlighting the intense drawdown of dZn by biota in this region to meet a high metabolic dZn demand.

Similar trends were observed for dZn : dP and dCd : dP, which exhibited shallow slopes within the upper ocean of the Ross Sea and Terra Nova Bay. Southern Ocean diatoms are known to have Zn : P uptake ratios that are up to an order of magnitude greater than the average for oceanic phytoplankton (Sieber et al., 2020; Twining and Baines, 2013; Vance et al., 2017). The increased presence of diatoms (as indicated by higher fucoxanthin concentrations) at the late stations within Terra Nova Bay therefore likely exacerbated the surface decoupling of dZn and dP due to their high dZn demand. The maximum uptake rates of 158, 115, and 89 $\mu\text{mol Zn L}^{-1} \text{ d}^{-1}$ measured in this study for the Amundsen Sea, Ross Sea, and Terra Nova Bay groups, respectively, contextualize the high Zn uptake rates hypothesized to contribute to the high dZn : dP uptake ratios observed in Southern Ocean diatoms. These rates are indicative of total potential biological uptake, likely influenced by a depleted labile Zn pool and residual of complexed Zn, which then results in low dZn : dP ratios in shallow waters.

Like dZn and dSi, dCd and dP concentrations are known to share strong correlations in both deep and surface seawater

(de Baar et al., 1994; Boyle, 1988; Boyle et al., 1976), with the vertical distribution of Cd controlled by phytoplankton uptake in surface waters and sinking of particulate organic matter and subsequent remineralization at depth. Observations of enhanced Cd uptake within the Fe-limited Southern Ocean (Cullen, 2006) are consistent with observations of increased Cd uptake by marine algal species under Fe limitation both in the field (Baars et al., 2014; Cullen et al., 2003; Cullen and Sherrell, 2005) and in cultures (Lane et al., 2009; Sunda and Huntsman, 2000), which is thought to be due to the increased use of Cd in biochemical processes or inadvertent uptake due to the upregulation of metal transporters (Cullen, 2006; Sunda and Huntsman, 2000). In these coastal regions, $dCd : dP$ had the same regional and depth trends as $dZn : dP$, further demonstrating their close biogeochemical association.

5 Conclusions

We have quantified the movement of the trace metals Zn and Cd from the dissolved to the particulate phase within the phytoplankton $> 3 \mu\text{m}$ size fraction collected in the Amundsen Sea, Ross Sea, and Terra Nova Bay of the Southern Ocean during austral summer 2017–2018. Our study adapts the stable Cd isotope tracer uptake method (Cox et al., 2014) to the measurement of Zn uptake and represents the first time series measurements of dZn and Zn uptake in a coastal environment during a bloom event. We have found that these high observed uptake rates were sufficient to draw down the otherwise abundant dZn inventory on seasonal timescales. Our analysis suggests that enhanced total biomass and low $p\text{CO}_2$ act as primary influences on ρZn and that high ρZn results in dynamic changes in the cycling of both Cd and Co as a consequence of high Zn demand. Low $dZn : Si$ slope values observed in the Ross Sea and Terra Nova Bay further highlighted the intense drawdown of dZn by biota to meet a high metabolic dZn demand. Overall, our study demonstrates that Zn demand is high and rapid enough to depress the inventory of Zn available to phytoplankton, suggesting that Zn has been overlooked as a dynamic limiting micronutrient in primary productivity modeling.

Data availability. CICLOPS (NBP18-01) conductivity–temperature–depth (CTD) hydrography data (including pressure, temperature, total dissolved oxygen, conductivity, fluorescence, and beam transmission; <https://doi.org/10.1575/1912/bco-dmo.783911.1>, DiTullio and Lee, 2020) and total dissolved metal, Zn and Cd uptake rate, macronutrient, and pigment datasets are available through the NSF Biological and Chemical Oceanography Data Management Office (BCO-DMO) repository (<https://doi.org/10.7284/907753>, Rolling Deck To Repository, 2018). Underway $p\text{CO}_2$ data collected during cruise NBP1801 are available through R2R at <https://doi.org/10.7284/139318> (DiTullio, 2017).

Supplement. The supplement related to this article is available online at: <https://doi.org/10.5194/bg-21-5685-2024-supplement>.

Author contributions. Conceptualization and analysis of the study was carried out by RMK and MAS. This work was supervised by MAS and GRDT. Funding was acquired by MAS and GRDT. RJC and DR contributed $d\text{Co}$ data and discussion. DMM, MRM, NLS, IS, and RBD aided in sampling and data collection. TJH contributed to analysis and discussion. RMK and MAS wrote the manuscript, with all co-authors contributing to reviewing and editing the manuscript.

Competing interests. The contact author has declared that none of the authors has any competing interests.

Disclaimer. Publisher's note: Copernicus Publications remains neutral with regard to jurisdictional claims made in the text, published maps, institutional affiliations, or any other geographical representation in this paper. While Copernicus Publications makes every effort to include appropriate place names, the final responsibility lies with the authors.

Acknowledgements. We thank the captain, crew, marine technicians, and science party of RVIB *Nathaniel B. Palmer* for their support and contributions to the success of the NBP18-01 cruise; Joe Jennings (OSU) for conducting macronutrient analyses; Lauren Lees for assistance with sampling; and Natalie Cohen for assistance in the operation of the seaFAST and application of the isotope dilution technique. Tristan J. Horner acknowledges support from the Woods Hole Oceanographic Institution's Ocean and Climate Innovation Accelerator program.

Financial support. This research has been supported by the National Science Foundation (grant nos. 2123055, 2125063, 1643684, 1924554, 2048774, NSF-PLR 1643845, and NSF-OPP 1644073) and the Simons Foundation.

Review statement. This paper was edited by Emilio Marañón and reviewed by Yeala Shaked and two anonymous referees.

References

- Arrigo, K. R., van Dijken, G. L., and Bushinsky, S.: Primary production in the Southern Ocean, 1997–2006, *J. Geophys. Res.*, 113, C08004, <https://doi.org/10.1029/2007JC004551>, 2008.
- Arrigo, K. R., Lowry, K. E., and van Dijken, G. L.: Annual changes in sea ice and phytoplankton in polynyas of the Amundsen Sea, Antarctica, *Deep-Sea Res. Pt. II*, 71–76, 5–15, <https://doi.org/10.1016/j.dsr2.2012.03.006>, 2012.
- Asper, V. L. and Smith, W. O.: Particle fluxes during austral spring and summer in the southern Ross Sea,

- Antarctica, *J. Geophys. Res.-Oceans*, 104, 5345–5359, <https://doi.org/10.1029/1998jc900067>, 1999.
- Baars, O. and Croot, P. L.: The speciation of dissolved zinc in the Atlantic sector of the Southern Ocean, *Deep-Sea Res. Pt. II*, 58, 2720–2732, <https://doi.org/10.1016/j.dsr2.2011.02.003>, 2011.
- Baars, O., Abouchami, W., Galer, S. J. G., Boye, M., and Croot, P. L.: Dissolved cadmium in the Southern Ocean: Distribution, speciation, and relation to phosphate, *Limnol. Oceanogr.*, 59, 385–399, <https://doi.org/10.4319/LO.2014.59.2.0385>, 2014.
- Bertrand, E. M., Saito, M. A., Rose, J. M., Riesselman, C. R., Lohan, M. C., Noble, A. E., Lee, P. A., and DiTullio, G. R.: Vitamin B₁₂ and iron colimitation of phytoplankton growth in the Ross Sea, *Limnol. Oceanogr.*, 52, 1079–1093, <https://doi.org/10.4319/lo.2007.52.3.1079>, 2007.
- Billler, D. V. and Bruland, K. W.: Analysis of Mn, Fe, Co, Ni, Cu, Zn, Cd, and Pb in seawater using the Nobias-chelate PA1 resin and magnetic sector inductively coupled plasma mass spectrometry (ICP-MS), *Mar. Chem.*, 130–131, 12–20, <https://doi.org/10.1016/j.marchem.2011.12.001>, 2012.
- Bishop, J. K. B. and Wood, T. J.: Year-round observations of carbon biomass and flux variability in the Southern Ocean, *Global Biogeochem. Cy.*, 23, GB2019, <https://doi.org/10.1029/2008GB003206>, 2009.
- Bown, J., Laan, P., Ossebaar, S., Bakker, K., Rozema, P., and de Baar, H. J. W.: Bioactive trace metal time series during Austral summer in Ryder Bay, Western Antarctic Peninsula, *Deep-Sea Res. Pt. II*, 139, 103–119, <https://doi.org/10.1016/j.dsr2.2016.07.004>, 2017.
- Boyle, E. A.: Cadmium: Chemical tracer of deepwater paleoceanography, *Paleoceanography*, 3, 471–489, <https://doi.org/10.1029/PA003i004p00471>, 1988.
- Boyle, E. A., Sclater, F., and Edmond, J. M.: On the marine geochemistry of cadmium, *Nature*, 263, 42–44, <https://doi.org/10.1038/263042a0>, 1976.
- Brand, L. E., Sunda, W. G., and Guillard, R. R. L.: Reduction of marine phytoplankton reproduction rates by copper and cadmium, *J. Exp. Mar. Biol. Ecol.*, 96, 225–250, [https://doi.org/10.1016/0022-0981\(86\)90205-4](https://doi.org/10.1016/0022-0981(86)90205-4), 1986.
- Bruland, K. W., Knauer, G. A., and Martin, J. H.: Zinc in north-east Pacific water, *Nature*, 271, 741–743, <https://doi.org/10.1038/271741a0>, 1978.
- Chmiel, R. J., Kell, R. M., Rao, D., Moran, D. M., DiTullio, G. R., and Saito, M. A.: Low cobalt inventories in the Amundsen and Ross seas driven by high demand for labile cobalt uptake among native phytoplankton communities, *Biogeosciences*, 20, 3997–4027, <https://doi.org/10.5194/bg-20-3997-2023>, 2023.
- Cox, A. D., Noble, A. E., and Saito, M. A.: Cadmium enriched stable isotope uptake and addition experiments with natural phytoplankton assemblages in the Costa Rica Upwelling Dome, *Mar. Chem.*, 166, 70–81, <https://doi.org/10.1016/j.marchem.2014.09.009>, 2014.
- Cramer, F.: Scientific colour maps, Zenodo [code], <https://doi.org/10.5281/zenodo.1243862>, 2023.
- Cullen, J. T.: On the nonlinear relationship between dissolved cadmium and phosphate in the modern global ocean: Could chronic iron limitation of phytoplankton growth cause the kink?, *Limnol. Oceanogr.*, 51, 1369–1380, <https://doi.org/10.4319/lo.2006.51.3.1369>, 2006.
- Cullen, J. T. and Sherrell, R. M.: Effects of dissolved carbon dioxide, zinc, and manganese on the cadmium to phosphorus ratio in natural phytoplankton assemblages, *Limnol. Oceanogr.*, 50, 1193–1204, <https://doi.org/10.4319/lo.2005.50.4.1193>, 2005.
- Cullen, J. T., Lane, T. W., Morel, F. M. M., and Sherrell, R. M.: Modulation of cadmium uptake in phytoplankton by seawater CO₂ concentration, *Nature*, 402, 165–167, <https://doi.org/10.1038/46007>, 1999.
- Cullen, J. T., Chase, Z., Coale, K. H., Fitzwater, S. E., and Sherrell, R. M.: Effect of iron limitation on the cadmium to phosphorus ratio of natural phytoplankton assemblages from the Southern Ocean, *Limnol. Oceanogr.*, 48, 1079–1087, <https://doi.org/10.4319/lo.2003.48.3.1079>, 2003.
- Cutter, G. A. and Bruland, K. W.: Rapid and noncontaminating sampling system for trace elements in global ocean surveys, *Limnol. Oceanogr.-Meth.*, 10, 425–436, <https://doi.org/10.4319/lom.2012.10.425>, 2012.
- Das, P., Samantaray, S., and Rout, G. R.: Studies on cadmium toxicity in plants: A review, *Environ. Pollut.*, 98, 29–36, [https://doi.org/10.1016/S0269-7491\(97\)00110-3](https://doi.org/10.1016/S0269-7491(97)00110-3), 1997.
- de Baar, H. J. W., Saager, P. M., Nolting, R. F., and van der Meer, J.: Cadmium versus phosphate in the world ocean, *Mar. Chem.*, 46, 261–281, [https://doi.org/10.1016/0304-4203\(94\)90082-5](https://doi.org/10.1016/0304-4203(94)90082-5), 1994.
- de Baar, H. J. W., van Heuven, S. M. A. C., Abouchami, W., Xue, Z., Galer, S. J. G., Rehkämper, M., Middag, R., and van Ooijen, J.: Interactions of dissolved CO₂ with cadmium isotopes in the Southern Ocean, *Mar. Chem.*, 195, 105–121, <https://doi.org/10.1016/j.marchem.2017.06.010>, 2017.
- DiTullio, G.: pCO₂ (LDEO pCO₂) data as collected during the cruise NBP1801, Ditullio/B-007; Dunbar/O-131; Saba/B-050, Rolling Deck to Repository (R2R) [data set], <https://doi.org/10.7284/139318>, 2017.
- DiTullio, G. and Lee, P.: Hydrographic data collected by CTD during RVIB Nathaniel B. Palmer cruise in the Ross Sea, Southern Ocean from 2017–2018, Version 1, Biological and Chemical Oceanography Data Management Office (BCO-DMO) [data set], <https://doi.org/10.1575/1912/bco-dmo.783911.1>, 2020.
- DiTullio, G. R. and Smith, W. O.: Relationship between dimethylsulfide and phytoplankton pigment concentrations in the Ross Sea, Antarctica, *Deep-Sea Res. Pt. I*, 42, 873–892, [https://doi.org/10.1016/0967-0637\(95\)00051-7](https://doi.org/10.1016/0967-0637(95)00051-7), 1995.
- DiTullio, G. R., Geesey, M. E., Leventer, A., and Lizotte, M. P.: Algal Pigment Ratios in the Ross Sea: Implications for Chemtax Analysis of Southern Ocean Data, in: *Biogeochemistry of the Ross Sea*, edited by: DiTullio, G. R. and Dunbar, R. B., <https://doi.org/10.1029/078ARS03>, 2003.
- DiTullio, G. R., Garcia, N., Riseman, S. F., and Sedwick, P. N.: Effects of iron concentration on pigment composition in Phaeocystis antarctica grown at low irradiance, *Biogeochemistry*, 83, 71–81, <https://doi.org/10.1007/s10533-007-9080-8>, 2007.
- Fitzwater, S. E., Johnson, K. S., Gordon, R. M., Coale, K. H., and Smith, W. O.: Trace metal concentrations in the Ross Sea and their relationship with nutrients and phytoplankton growth, *Deep-Sea Res. Pt. II*, 47, 3159–3179, [https://doi.org/10.1016/S0967-0645\(00\)00063-1](https://doi.org/10.1016/S0967-0645(00)00063-1), 2000.
- Gerringa, L. J. A., Alderkamp, A.-C., van Dijken, G., Laan, P., Middag, R., and Arrigo, K. R.: Dissolved Trace Metals in the Ross Sea, *Frontiers in Marine Science*, 7, 577098, <https://doi.org/10.3389/fmars.2020.577098>, 2020.

- Giordano, R., Lombardi, G., Ciaralli, L., Beccaloni, E., Sepe, A., Ciprotti, M., and Costantini, S.: Major and trace elements in sediments from Terra Nova Bay, Antarctica, *Sci. Total Environ.*, 227, 29–40, [https://doi.org/10.1016/S0048-9697\(98\)00402-1](https://doi.org/10.1016/S0048-9697(98)00402-1), 1999.
- Haas, C. E., Rodionov, D. A., Kropat, J., Malasarn, D., Merchant, S. S., and de Crécy-Lagard, V.: A subset of the diverse COG0523 family of putative metal chaperones is linked to zinc homeostasis in all kingdoms of life, *BMC Genomics*, 10, 470, <https://doi.org/10.1186/1471-2164-10-470>, 2009.
- Hopwood, M. J., Carroll, D., Höfer, J., Achterberg, E. P., Meire, L., Le Moigne, F. A. C., Bach, L. T., Eich, C., Sutherland, D. A., and González, H. E.: Highly variable iron content modulates iceberg-ocean fertilisation and potential carbon export, *Nat. Commun.*, 10, 5261, <https://doi.org/10.1038/s41467-019-13231-0>, 2019.
- Horner, T. J., Lee, R. B. Y., Henderson, G. M., and Rickaby, R. E. M.: Nonspecific uptake and homeostasis drive the oceanic cadmium cycle, *P. Natl. Acad. Sci. USA*, 110, 2500–2505, <https://doi.org/10.1073/pnas.1213857110>, 2013.
- Horner, T. J., Little, S. H., Conway, T. M., Farmer, J. R., Hertzberg, J. E., Janssen, D. J., Lough, A. J. M., McKay, J. L., Tessin, A., Galer, S. J. G., Jaccard, S. L., Lacan, F., Paytan, A., Wuttig, K., and GEOTRACES–PAGES Biological Productivity Working Group Members: Bioactive Trace Metals and Their Isotopes as Paleoproductivity Proxies: An Assessment Using GEOTRACES–Era Data, *Global Biogeochem. Cy.*, 35, e2020GB006814, <https://doi.org/10.1029/2020GB006814>, 2021.
- Hutchins, D. and Bruland, K.: Grazer-mediated regeneration and assimilation of Fe, Zn and Mn from planktonic prey, *Mar. Ecol. Prog. Ser.*, 110, 259–269, <https://doi.org/10.3354/meps110259>, 1994.
- Hutchins, D. A. and Bruland, K. W.: Fe, Zn, Mn and N transfer between size classes in a coastal phytoplankton community: Trace metal and major nutrient recycling compared, *J. Mar. Res.*, 53, 297–313, 1995.
- Hutchins, D. A., Wang, W. X., Schmidt, M. A., and Fisher, N. S.: Dual-labeling techniques for trace metal biogeochemical investigations in aquatic plankton communities, *Aquat. Microb. Ecol.*, 19, 129–138, <https://doi.org/10.3354/ame019129>, 1999.
- Irving, B. H. and Williams, R. J. P.: The Stability of Transition-metal Complexes, *J. Chem. Soc.*, 3192–3210, <https://doi.org/10.1039/JR9530003192>, 1953.
- Jackson, S. L., Spence, J., Janssen, D. J., Ross, A. R. S., and Cullen, J. T.: Determination of Mn, Fe, Ni, Cu, Zn, Cd and Pb in seawater using offline extraction and triple quadrupole ICP-MS/MS, *J. Anal. Atom. Spectrom.*, 33, 304–313, <https://doi.org/10.1039/c7ja00237h>, 2018.
- Kato, T., Nakamura, S., and Morita, M.: Determination of Nickel, Copper, Zinc, Silver, Cadmium and Lead in Seawater by Isotope Dilution Inductively Coupled Plasma Mass Spectrometry, *Anal. Sci.*, 6, 623–626, <https://doi.org/10.2116/analsci.6.623>, 1990.
- Kell, R. M., Subhas, A. V., Schanke, N. L., Lees, L. E., Chmiel, R. J., Rao, D., Brisbin, M. M. M., Moran, D. M., McIlvin, M. R., Bolinesi, F., Mangoni, O., Casotti, R., Balestra, C., Horner, T., Dunbar, R. B., Allen, A. E., DiTullio, G. R., and Saito, M. A.: Zinc stimulation of phytoplankton in a low carbon dioxide, coastal Antarctic environment, *bioRxiv* [preprint], <https://doi.org/10.1101/2023.11.05.565706>, 5 November 2023.
- Kellogg, R. M., Moosburner, M. A., Cohen, N. R., Hawco, N. J., McIlvin, M. R., Moran, D. M., DiTullio, G. R., Subhas, A. V., Allen, A. E., and Saito, M. A.: Adaptive responses of marine diatoms to zinc scarcity and ecological implications, *Nat. Commun.*, 13, 1995, <https://doi.org/10.1038/s41467-022-29603-y>, 2022.
- Lane, E. S., Semeniuk, D. M., Strzepek, R. F., Cullen, J. T., and Maldonado, M. T.: Effects of iron limitation on intracellular cadmium of cultured phytoplankton: Implications for surface dissolved cadmium to phosphate ratios, *Mar. Chem.*, 115, 155–162, <https://doi.org/10.1016/j.marchem.2009.07.008>, 2009.
- Lane, T. W., Saito, M. A., George, G. N., Pickering, I. J., Prince, R. C., and Morel, F. M. M.: A cadmium enzyme from a marine diatom, *Nature*, 435, 42–42, <https://doi.org/10.1038/435042a>, 2005.
- Latour, P., Wuttig, K., van der Merwe, P., Strzepek, R. F., Gault-Ringold, M., Townsend, A. T., Holmes, T. M., Corkill, M., and Bowie, A. R.: Manganese biogeochemistry in the Southern Ocean, from Tasmania to Antarctica, *Limnol. Oceanogr.*, 66, 2547–2562, <https://doi.org/10.1002/lno.11772>, 2021.
- Lee, J. and Morel, F.: Replacement of zinc by cadmium in marine phytoplankton, *Mar. Ecol. Prog. Ser.*, 127, 305–309, <https://doi.org/10.3354/meps127305>, 1995.
- Lee, J. G., Roberts, S. B., and Morel, F. M. M.: Cadmium: A nutrient for the marine diatom *Thalassiosira weissflogii*, *Limnol. Oceanogr.*, 40, 1056–1063, <https://doi.org/10.4319/lo.1995.40.6.1056>, 1995.
- Lohan, M. C., Statham, P. J., and Crawford, D. W.: Total dissolved zinc in the upper water column of the subarctic North East Pacific, *Deep-Sea Res. Pt. II*, 49, 5793–5808, [https://doi.org/10.1016/S0967-0645\(02\)00215-1](https://doi.org/10.1016/S0967-0645(02)00215-1), 2002.
- Martin, J. H.: Glacial-interglacial CO₂ change: The Iron Hypothesis, *Paleoceanography*, 5, 1–13, <https://doi.org/10.1029/PA005i001p00001>, 1990.
- Middag, R., Baar, H. J. W., and Bruland, K. W.: The relationships between dissolved zinc and major nutrients phosphate and silicate along the GEOTRACES GA02 transect in the West Atlantic Ocean, *Global Biogeochem. Cy.*, 33, 63–84, <https://doi.org/10.1029/2018GB006034>, 2019.
- Morel, F. M. M., Reinfelder, J. R., Roberts, S. B., Chamberlain, C. P., Lee, J. G., and Yee, D.: Zinc and carbon co-limitation of marine phytoplankton, *Nature*, 369, 740–742, <https://doi.org/10.1038/369740A0>, 1994.
- Morel, F. M. M., Milligan, A. J., and Saito, M. A.: 8.5 - Marine Bioinorganic Chemistry: The Role of Trace Metals in the Oceanic Cycles of Major Nutrients, in: *Treatise on Geochemistry (Second Edition)*, edited by: Holland, H. D. and Turekian, K. K., Elsevier, Oxford, 123–150 <https://doi.org/10.1016/B978-0-08-095975-7.00605-7>, 2013.
- Morel, F. M. M., Lam, P. J., and Saito, M. A.: Trace metal substitution in marine phytoplankton, *Annu. Rev. Earth Pl. Sc.*, 48, 491–517, <https://doi.org/10.1146/annurev-earth-053018-060108>, 2020.
- Noble, A. E., Lamborg, C. H., Ohnemus, D. C., Lam, P. J., Goepfert, T. J., Measures, C. I., Frame, C. H., Casciotti, K. L., DiTullio, G. R., Jennings, J., and Saito, M. A.: Basin-scale inputs of cobalt, iron, and manganese from the Benguela-Angola front to the South Atlantic Ocean, *Limnol. Oceanogr.*, 57, 989–1010, <https://doi.org/10.4319/lo.2012.57.4.0989>, 2012.

- Noble, A. E., Moran, D. M., Allen, A. E., and Saito, M. A.: Dissolved and particulate trace metal micronutrients under the McMurdo Sound seasonal sea ice: basal sea ice communities as a capacitor for iron, *Front. Chem.*, 1, 25, <https://doi.org/10.3389/fchem.2013.00025>, 2013.
- Ohnemus, D. C., Rauschenberg, S., Cutter, G. A., Fitzsimmons, J. N., Sherrell, R. M., and Twining, B. S.: Elevated trace metal content of prokaryotic communities associated with marine oxygen deficient zones, *Limnol. Oceanogr.*, 62, 3–25, <https://doi.org/10.1002/lno.10363>, 2017.
- Oldham, V. E., Chmiel, R., Hansel, C. M., DiTullio, G. R., Rao, D., and Saito, M.: Inhibited Manganese Oxide Formation Hinders Cobalt Scavenging in the Ross Sea, *Global Biogeochem. Cy.*, 35, e2020GB006706, <https://doi.org/10.1029/2020GB006706>, 2021.
- Park, H., Song, B., and Morel, F. M. M.: Diversity of the cadmium-containing carbonic anhydrase in marine diatoms and natural waters, *Environ. Microbiol.*, 9, 403–413, <https://doi.org/10.1111/j.1462-2920.2006.01151.x>, 2007.
- Park, H., McGinn, P. J., and Morel, F. M. M.: Expression of cadmium carbonic anhydrase of diatoms in seawater, *Aquat. Microb. Ecol.*, 51, 183–193, <https://doi.org/10.3354/ame01192>, 2008.
- Person, R., Vancoppenolle, M., Aumont, O., and Malsang, M.: Continental and Sea Ice Iron Sources Fertilize the Southern Ocean in Synergy, *Geophys. Res. Lett.*, 48, e2021GL094761, <https://doi.org/10.1029/2021GL094761>, 2021.
- Planquette, H., Sherrell, R. M., Stammerjohn, S., and Field, M. P.: Particulate iron delivery to the water column of the Amundsen Sea, *Antarctica, Mar. Chem.*, 153, 15–30, <https://doi.org/10.1016/j.marchem.2013.04.006>, 2013.
- Price, N. M. and Morel, F. M. M.: Cadmium and cobalt substitution for zinc in a marine diatom, *Nature*, 344, 658–660, <https://doi.org/10.1038/344658a0>, 1990.
- Rapp, L., Schlosser, C., Rusiecka, D., Gledhill, M., and Achterberg, E. P.: Automated preconcentration of Fe, Zn, Cu, Ni, Cd, Pb, Co, and Mn in seawater with analysis using high-resolution sector field inductively-coupled plasma mass spectrometry, *Anal. Chim. Acta*, 976, 1–13, <https://doi.org/10.1016/j.aca.2017.05.008>, 2017.
- Rolling Deck To Repository: Cruise NBP1801 on RV Nathaniel B. Palmer, <https://doi.org/10.7284/907753>, 2018.
- Roshan, S., DeVries, T., Wu, J., and Chen, G.: The Internal Cycling of Zinc in the Ocean, *Global Biogeochem. Cy.*, 32, 1833–1849, <https://doi.org/10.1029/2018GB006045>, 2018.
- Rudge, J. F., Reynolds, B. C., and Bourdon, B.: The double spike toolbox, *Chem. Geol.*, 265, 420–431, <https://doi.org/10.1016/j.chemgeo.2009.05.010>, 2009.
- Saito, M. A. and Goepfert, T. J.: Zinc-cobalt colimitation of *Phaeocystis antarctica*, *Limnol. Oceanogr.*, 53, 266–275, <https://doi.org/10.4319/lno.2008.53.1.0266>, 2008.
- Sedwick, P. N. and DiTullio, G. R.: Regulation of algal blooms in Antarctic shelf waters by the release of iron from melting sea ice, *Geophys. Res. Lett.*, 24, 2515–2518, <https://doi.org/10.1029/97GL02596>, 1997.
- Sedwick, P. N., Di Tullio, G. R., and Mackey, D. J.: Iron and manganese in the Ross Sea, Seasonal iron limitation in Antarctic, *J. Geophys. Res.-Oceans*, 105, 11321–11336, <https://doi.org/10.1029/2000JC000256>, 2000.
- Sedwick, P. N., Marsay, C. M., Sohst, B. M., Aguilar-Islas, A. M., Lohan, M. C., Long, M. C., Arrigo, K. R., Dunbar, R. B., Saito, M. A., Smith, W. O., and DiTullio, G. R.: Early season depletion of dissolved iron in the Ross Sea polynya: Implications for iron dynamics on the Antarctic continental shelf, *J. Geophys. Res.*, 116, C12019, <https://doi.org/10.1029/2010JC006553>, 2011.
- Shaked, Y., Xu, Y., Leblanc, K., and Morel, F. M. M.: Zinc availability and alkaline phosphatase activity in *Emiliania huxleyi*: Implications for Zn-P co-limitation in the ocean, *Limnol. Oceanogr.*, 51, 299–309, <https://doi.org/10.4319/lno.2006.51.1.0299>, 2006.
- Sieber, M., Conway, T. M., de Souza, G. F., Hassler, C. S., Ellwood, M. J., and Vance, D.: Cycling of zinc and its isotopes across multiple zones of the Southern Ocean: Insights from the Antarctic Circumnavigation Expedition, *Geochim. Cosmochim. Ac.*, 268, 310–324, <https://doi.org/10.1016/j.gca.2019.09.039>, 2020.
- Sohrin, Y., Urushihara, S., Nakatsuka, S., Kono, T., Higo, E., Minami, T., Norisuye, K., and Umetani, S.: Multielemental determination of GEOTRACES key trace metals in seawater by ICPMS after preconcentration using an ethylenediamine-triacetic acid chelating resin, *Anal. Chem.*, 80, 6267–6273, <https://doi.org/10.1021/ac800500f>, 2008.
- St-Laurent, P., Yager, P. L., Sherrell, R. M., Stammerjohn, S. E., and Dinniman, M. S.: Pathways and supply of dissolved iron in the Amundsen Sea (Antarctica), *J. Geophys. Res.-Oceans*, 122, 7135–7162, <https://doi.org/10.1002/2017JC013162>, 2017.
- Sunda, W. G. and Huntsman, S. A.: Feedback interactions between zinc and phytoplankton in seawater, *Limnol. Oceanogr.*, 37, 25–40, <https://doi.org/10.4319/lno.1992.37.1.0025>, 1992.
- Sunda, W. G. and Huntsman, S. A.: Cobalt and zinc interreplacement in marine phytoplankton: Biological and geochemical implications, *Limnol. Oceanogr.*, 40, 1404–1417, <https://doi.org/10.4319/lno.1995.40.8.1404>, 1995.
- Sunda, W. G. and Huntsman, S. A.: Antagonisms between cadmium and zinc toxicity and manganese limitation in a coastal diatom, *Limnol. Oceanogr.*, 41, 373–387, <https://doi.org/10.4319/lno.1996.41.3.0373>, 1996.
- Sunda, W. G. and Huntsman, S. A.: Control of Cd Concentrations in a Coastal Diatom by Interactions among Free Ionic Cd, Zn, and Mn in Seawater, *Environ. Sci. Technol.*, 32, 2961–2968, <https://doi.org/10.1021/es980271y>, 1998a.
- Sunda, W. G. and Huntsman, S. A.: Processes regulating cellular metal accumulation and physiological effects: Phytoplankton as model systems, *Sci. Total Environ.*, 219, 165–181, [https://doi.org/10.1016/S0048-9697\(98\)00226-5](https://doi.org/10.1016/S0048-9697(98)00226-5), 1998b.
- Sunda, W. G. and Huntsman, S. A.: Effect of Zn, Mn, and Fe on Cd accumulation in phytoplankton: Implications for oceanic Cd cycling, *Limnol. Oceanogr.*, 45, 1501–1516, <https://doi.org/10.4319/lno.2000.45.7.1501>, 2000.
- Tan, D., Xu, W., Zhu, Z., Li, S., Wu, G., and Qin, H.: Optimizing the ratio of the spike to sample for isotope dilution analysis: a case study with selenium isotopes, *Acta Geochimica*, 39, 192–202, <https://doi.org/10.1007/s11631-019-00390-6>, 2020.
- Taylor, S. R. and McLennan, S. M.: *The Continental Crust: Its Composition and Evolution*, Blackwell Scientific Publications, Oxford, 312 pp., ISBN 0 632 01148 3, 1985.

- Twining, B. S. and Baines, S. B.: The trace metal composition of marine phytoplankton, *Annu. Rev. Mar. Sci.*, 5, 191–215, <https://doi.org/10.1146/annurev-marine-121211-172322>, 2013.
- Vance, D., Little, S. H., De Souza, G. F., Khatiwala, S., Lohan, M. C., and Middag, R.: Silicon and zinc biogeochemical cycles coupled through the Southern Ocean, *Nat. Geosci.*, 10, 202–206, <https://doi.org/10.1038/ngeo2890>, 2017.
- Weber, T., John, S., Tagliabue, A., and DeVries, T.: Biological uptake and reversible scavenging of zinc in the global ocean, *Science*, 361, 72–76, <https://doi.org/10.1126/science.aaP8532>, 2018.
- Wright, S. W., van den Enden, R. L., Pearce, I., Davidson, A. T., Scott, F. J., and Westwood, K. J.: Phytoplankton community structure and stocks in the Southern Ocean (30–80° E) determined by CHEMTAX analysis of HPLC pigment signatures, *Deep-Sea Res. Pt. II*, 57, 758–778, <https://doi.org/10.1016/j.dsr2.2009.06.015>, 2010.
- Wu, J. and Boyle, E. A.: Determination of iron in seawater by high-resolution isotope dilution inductively coupled plasma mass spectrometry after Mg(OH)₂ coprecipitation, *Anal. Chim. Acta*, 367, 183–191, [https://doi.org/10.1016/S0003-2670\(98\)00145-7](https://doi.org/10.1016/S0003-2670(98)00145-7), 1998.
- Wuttig, K., Townsend, A. T., van der Merwe, P., Gault-Ringold, M., Holmes, T., Schallenberg, C., Latour, P., Tonnard, M., Rijkenberg, M. J. A., Lannuzel, D., and Bowie, A. R.: Critical evaluation of a seaFAST system for the analysis of trace metals in marine samples, *Talanta*, 197, 653–668, <https://doi.org/10.1016/j.talanta.2019.01.047>, 2019.
- Xu, Y., Tang, D., Shaked, Y., and Morel, F. M. M.: Zinc, cadmium, and cobalt interreplacement and relative use efficiencies in the coccolithophore *Emiliania huxleyi*, *Limnol. Oceanogr.*, 52, 2294–2305, <https://doi.org/10.4319/lo.2007.52.5.2294>, 2007.
- Zhao, Y., Vance, D., Abouchami, W., and de Baar, H. J. W.: Biogeochemical cycling of zinc and its isotopes in the Southern Ocean, *Geochim. Cosmochim. Ac.*, 125, 653–672, <https://doi.org/10.1016/j.gca.2013.07.045>, 2014.